Supporting Information for

Phosphorus chirality assignment and solution dynamics of lanthanide(III) complexes of a monomethylphosphinate analogue of H_4dota: A multinuclear NMR and DFT study.

Adam Svítok,[a] Carlos Platas-Iglesias,[b] Jan Kotek,[a] Petr Hermann[a]*

[a]Department of Inorganic Chemistry, Faculty of Science, Charles University, Hlavova 2030, 12843 Prague 2, Czech Republic. Tel: +420-22195-1263, e-mail: petrh@natur.cuni.cz

[b]Universidade da Coruña, Centro Interdisciplinar de Química e Bioloxía (CICA) and Departamento de Química, Facultade de Ciencias, 15071, A Coruña, Galicia, Spain.

Content:

Discussion of solid-state structures

Solid-state structure of H_4do3ap^{Me}

The molecular structure of zwitter-ionic H_4do3ap^{Me} is shown in **Figure S1**. The structure is disordered into two positions where methylphosphinate group and the neighbouring carboxylate group interchange, with relative occupancy of 88:12 %; only the more abundant molecular structure is shown for clarity. In this zwitterionic structure, two opposite nitrogen atoms and the two neighbouring carboxylate groups are protonated. Protonation of macrocycle amino groups locks the ring conformation in (3,3,3,3)-B conformation typical for H_4dota-like ligands[1]. The rather unusual protonation of carboxylates in *cis* position is a result of the stabilisation of the crystal packing by very strong hydrogen bonds (ca 2.5 Å) between the protonated carboxylic pendant arms and oxygen atoms of deprotonated methylphosphinate or carboxylate groups, respectively. Each ligand molecule thus connects to two neighbouring molecules. The remaining oxygen atoms of deprotonated pendants serve as acceptors of hydrogen atoms of water molecules of crystallisation (**Figure S2**).

Figure S1. Molecular structures of zwitter-ionic H_4do3ap^{Me} found in the crystal structure of H_4do3ap^{Me}·3H_2O. For simplicity, carbon-bound hydrogen atoms are omitted, and only the more abundant positions of the disordered pendant groups are shown. Intramolecular hydrogen bonds are shown in turquoise.

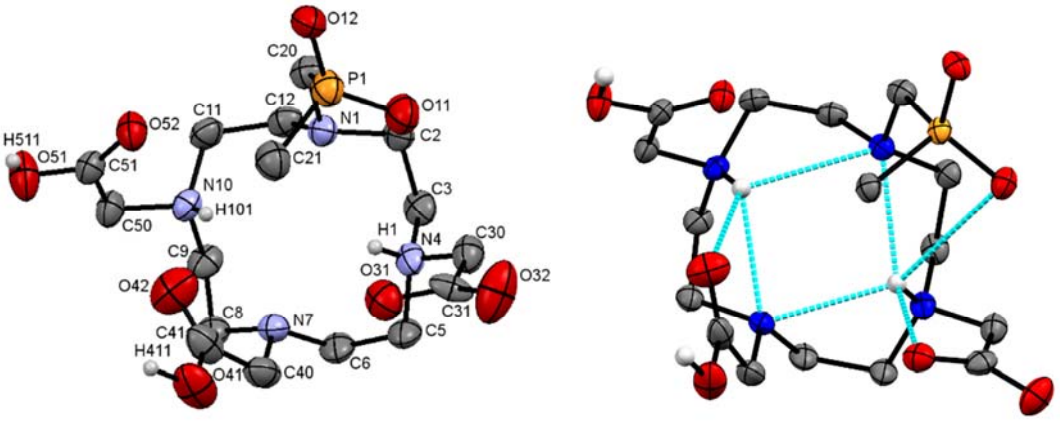

Figure S2. A motif of intermolecular hydrogen bonds (turquoise) found in the crystal structure of H_4do3ap^{Me}·3H_2O. The central ligand molecule connects to four neighbouring molecules through strong hydrogen bonds between the protonated and unprotonated pendant arms. From individual neighbouring ligand molecules, only the respective pendant arm including the pivot nitrogen atoms is shown for clarity.

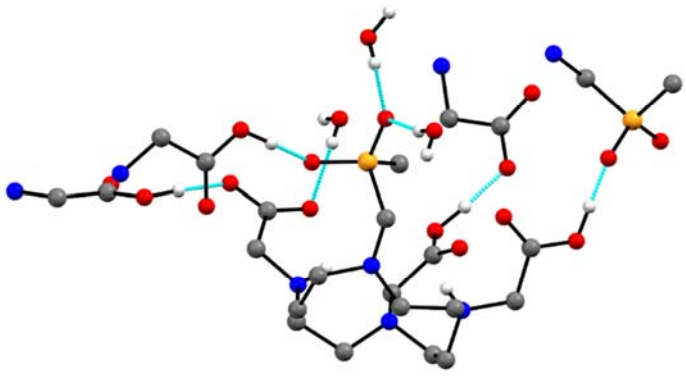

Solid-state structures of [Yb(DO3AP^{Me})]$^-$ and [Yb(DO3AP^{OEt})]$^-$ complexes

Molecular structures of the [Yb(do3ap^{Me})]$^-$ and [Yb(do3ap^{OEt})]$^-$ anions found in the solid-state structures of [Li(H_2O)$_3$][Yb(do3ap^{Me})]·H_2O and [Li(H_2O)$_3$][Yb(do3ap^{OEt})]·H_2O, respectively, are shown in **Figure S3**. Molecules in both crystal structures form an enantiomeric pair in the unit cell where the [Yb(do3ap^{Me})]$^-$ and [Yb(do3ap^{OEt})]$^-$ are forming the *R*-Λλλλλ/S-Δδδδδ (*v*-TSA′) and *S*-Λλλλλ/*R*-Δδδδδ (*h*-TSA′) pairs, respectively. Structures do not contain any coordinated water molecule (see also the main text). Selected distances and angles in the structure are shown in **Table S1**.

Figure S3. Molecular structure of the [Yb(do3ap^{Me})]$^-$ anion found in the solid-state structure of [Li(H_2O)$_3$][Yb(do3ap^{Me})]·H_2O (left) and molecular structure of the [Yb(do3ap^{OEt})]$^-$ anion found in the solid-state structure of [Li(H_2O)$_3$][Yb(do3ap^{Me})]·H_2O (right), with atom labelling scheme. Hydrogen atoms are not shown for the sake of clarity. Only one enantiomer of each enantiomeric pair is depicted: *R*-Λλλλλ and *S*-Λλλλλ for [Yb(do3ap^{Me})]$^-$ and [Yb(do3ap^{OEt})]$^-$, respectively.

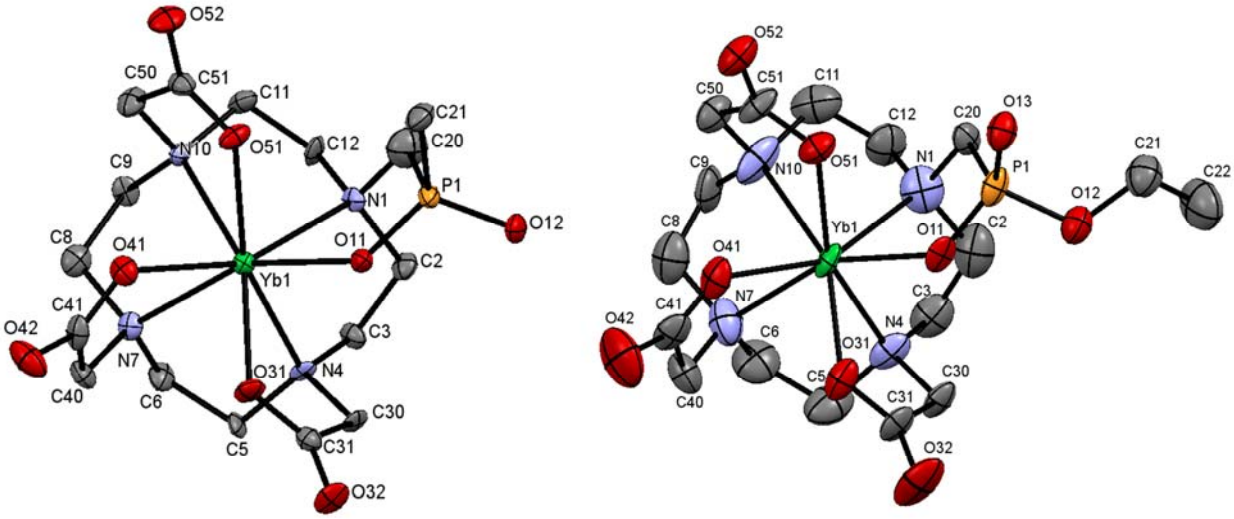

Table S1. Selected structural parameters of the solid-state structures of $[Yb(do3ap^{Me})]^-$ and $[Yb(do3ap^{OEt})]^-$. The atom numbering is shown in **Figure S3**.

Parameters	$[Li(H_2O)_3][Yb(do3ap^{Me})]\cdot H_2O$	$[Li(H_2O)_3][Yb(do3ap^{OEt})]\cdot H_2O$
Distances (Å)		
Yb–N1	2.573(8)	2.552(15)
Yb–N4	2.542(8)	2.498(12)
Yb–N7	2.518(9)	2.526(13)
Yb–N10	2.533(8)	2.529(14)
Yb–O11	2.212(7)	2.243(9)
Yb–O31	2.287(7)	2.255(11)
Yb–O41	2.273(7)	2.272(10)
Yb–O51	2.300(7)	2.258(10)
NQ···OQ [a]	2.528	2.512
Yb···N_4-plane [b]	1.482(4)	1.479(7)
Yb···O_4-plane [c]	1.046(4)	1.034(5)
O11···O_3-plane [d]	0.32(2)	0.27(2)
Angles (°)		
NQ···Yb···OQ [a]	176.97	177.50
N1···NQ···OQ···O11 [a]	27.4	28.4
N4···NQ···OQ···O31 [a]	26.2	28.1
N7···NQ···OQ···O41 [a]	26.7	27.6
N10···NQ···OQ···O51 [a]	26.3	28.9
O11–Yb–O41	119.7(3)	121.5(4)
O31–Yb–O51	130.1(3)	129.4(4)
N_4-plane···O_4-plane [b,c]	2.1(3)	2.6(4)

[a]The NQ and OQ are centroids of the O_4- and N_4-planes,[b,c] respectively. [b]The N_4-plane is the least-squares plane defined by macrocycle nitrogen atoms N1, N4, N7 and N10. [c]The O_4-plane is a least-squares plane defined by the coordinated pendant arm oxygen atoms O11, O31, O41 and O51. [d]The O_3-plane is the least-squares plane defined by the coordinated oxygen atoms of carboxylate pendant arms O31, O41 and O51.

NMR spectra of [Ln(do3ap^{Me})]$^{-}$

Figure S4. The ^{1}H NMR spectra of "axial proton" signals in paramagnetic [Ln(do3ap^{Me})]$^{-}$.

The spectra were measured in D_2O (pD ~6.5, t = 5 °C, $\nu(^{1}H)$ = 600 MHz) and the diastereoisomers are assigned by analogy with [Ln(dota)]$^{-}$. Only the best assignable signals of "axial protons" (for definition, see SI of a reference[1]) are shown for simplicity.

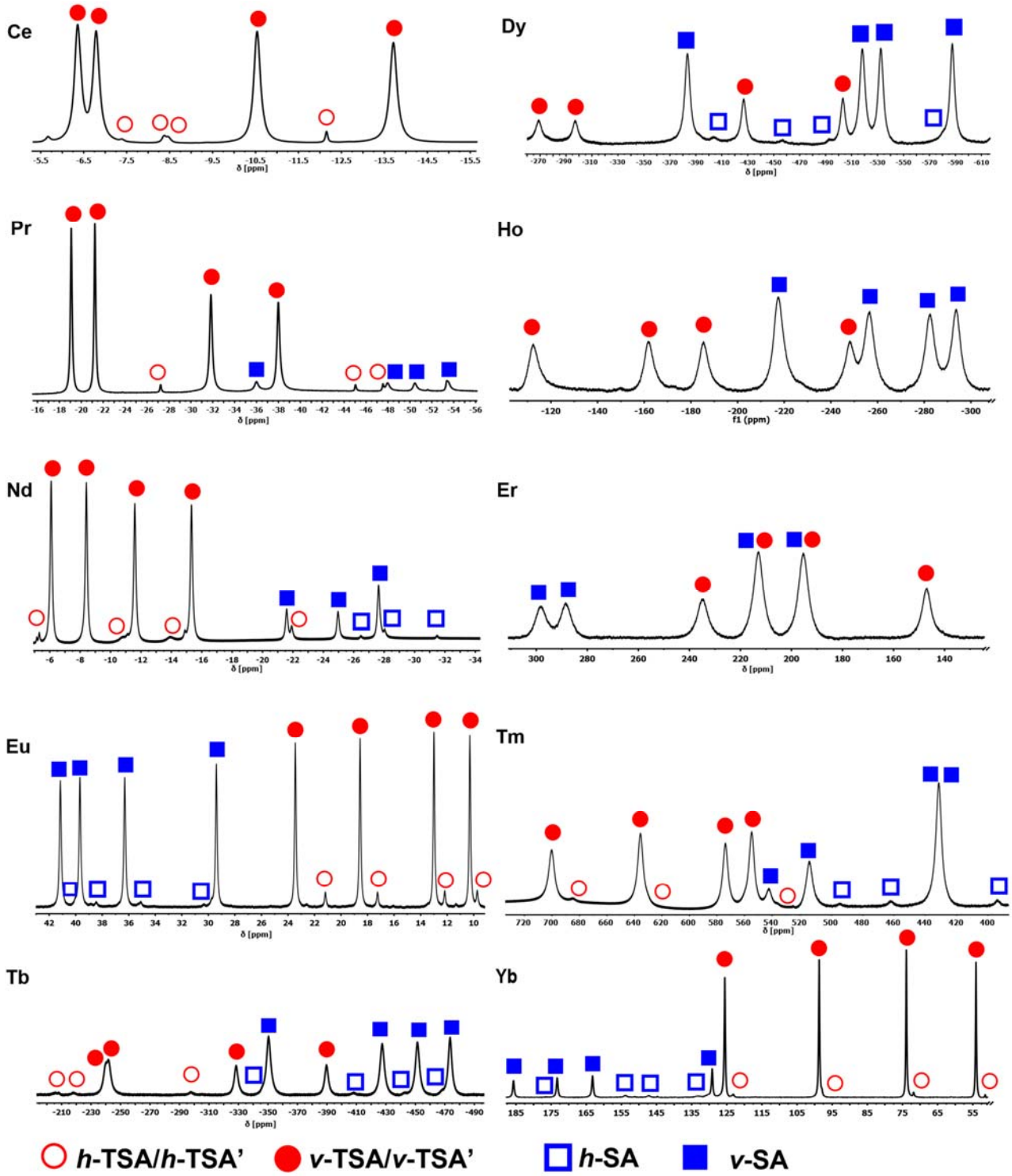

Figure S5. The ^{1}H NMR spectra of diamagnetic [La/Lu(do3ap^{Me})]$^{-}$ and weakly paramagnetic [Sm(do3ap^{Me})]$^{-}$.

The spectra were measured in D_2O (pD ~6.5, t = 5 °C and $\nu(^{1}H)$ = 600 MHz). The resolution is too low to assign the signals due to their overlap.

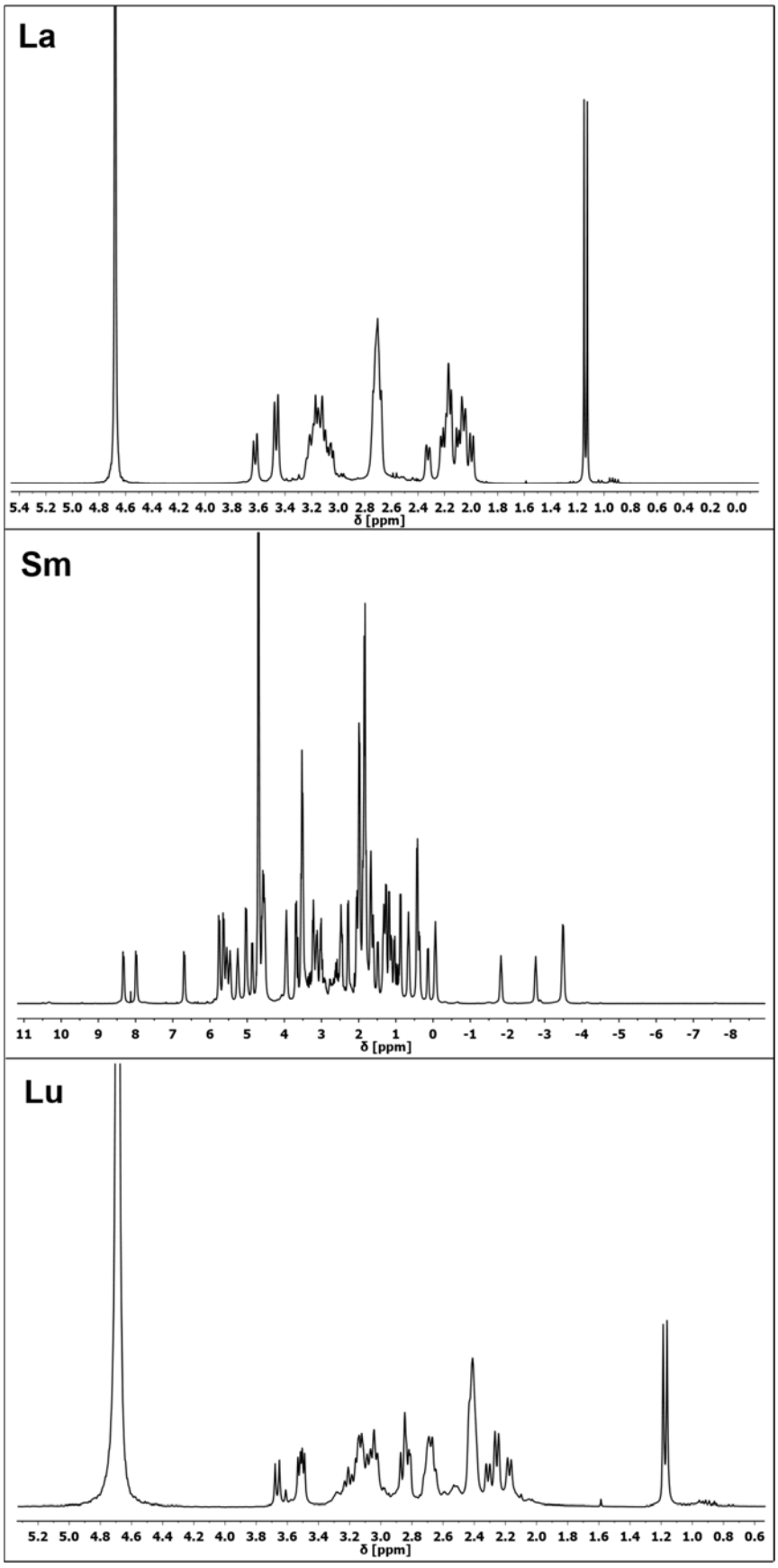

Figure S6. The ^{31}P NMR spectra of $[Ln(do3ap^{Me})]^-$ complexes.

The spectra were measured in D_2O (pD ~6.5, t = 5 °C, $\nu(^{31}P)$ = 243 MHz) and the diastereoisomers were assigned by comparing relative integral intensities with ^{1}H NMR spectra.

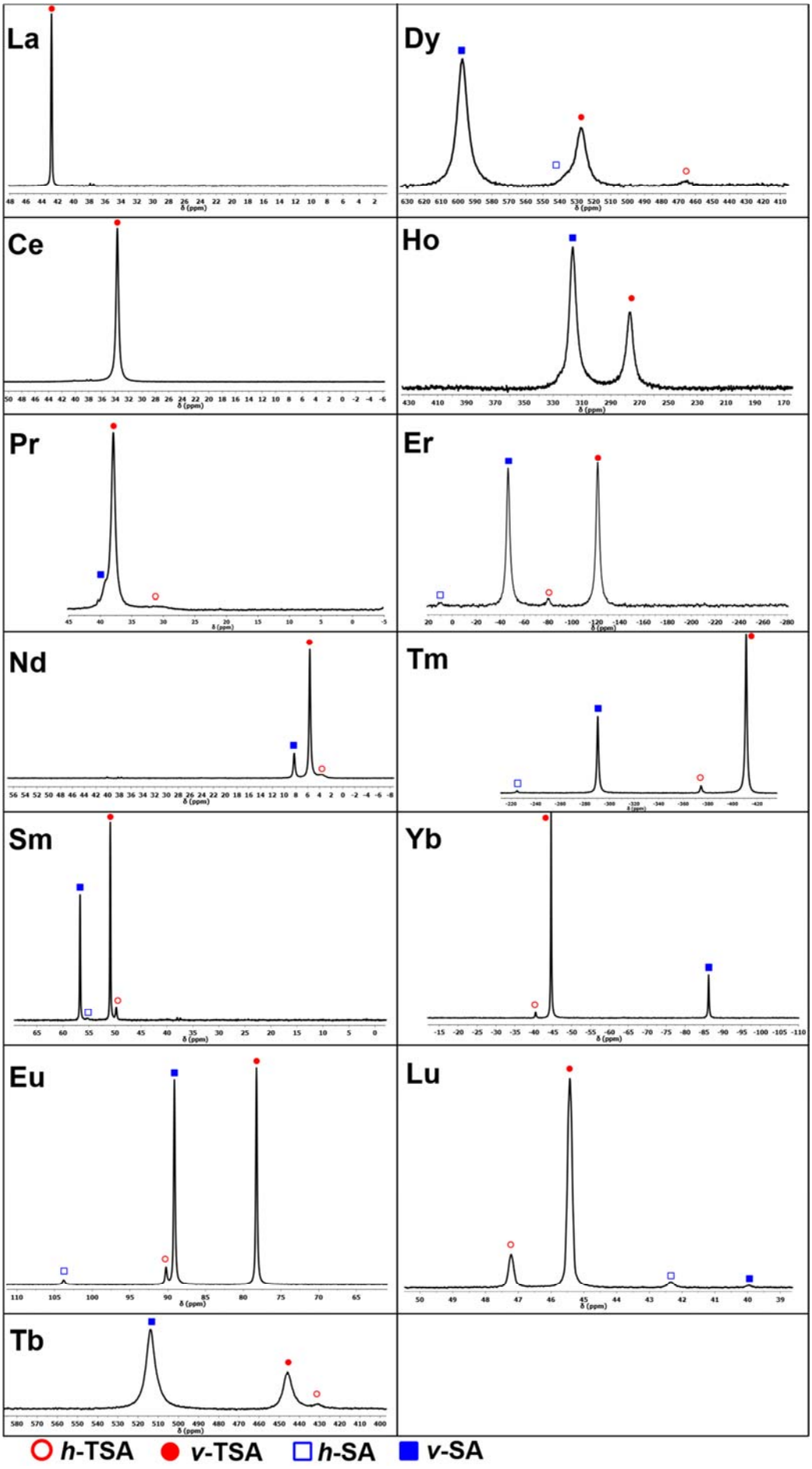

Figure S7. The ^{17}O NMR spectra of $[Ln(do3ap^{Me})]^-$ (Ln = La, Ce, Sm, Lu) complexes in D_2O (pD ~6.5, t = 5 °C $\nu(^{17}O)$ = 81 MHz).

Signals are assigned to coordinated and non-coordinated oxygen atoms. Due to coalescence, signals of different diastereoisomers are not resolved. The most intensive signal is the signal of $H_2{}^{17}O$ (0 ppm).

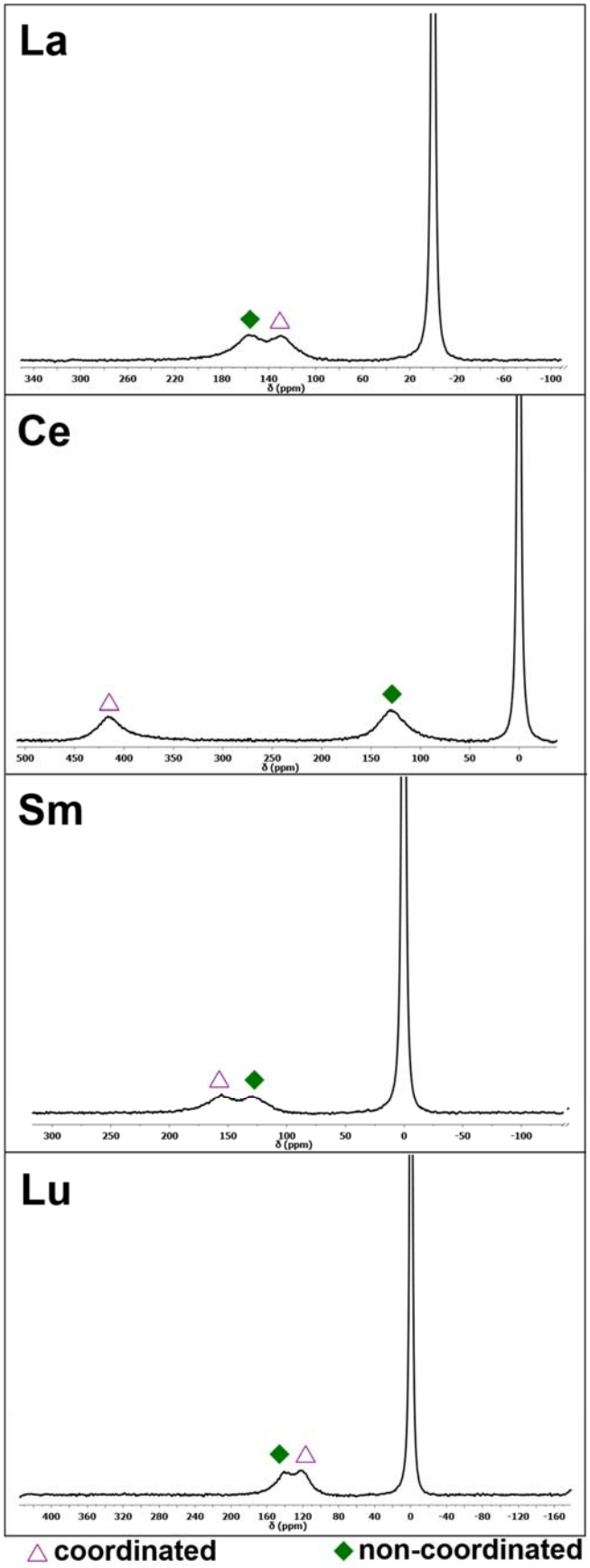

Figure S8. The ^{17}O NMR spectra of non-coordinated oxygen atom signals of some paramagnetic $[Ln(do3ap^{Me})]^{-}$.

The spectra were measured in D_2O (pD ~6.5, t = 5 °C, $\nu(^{17}O)$ = 81 MHz). Signals of different diastereoisomers are not resolved due to coalescence or could not be assigned due to overlap. The most intensive signal is the signal of $H_2{}^{17}O$ (0 ppm).

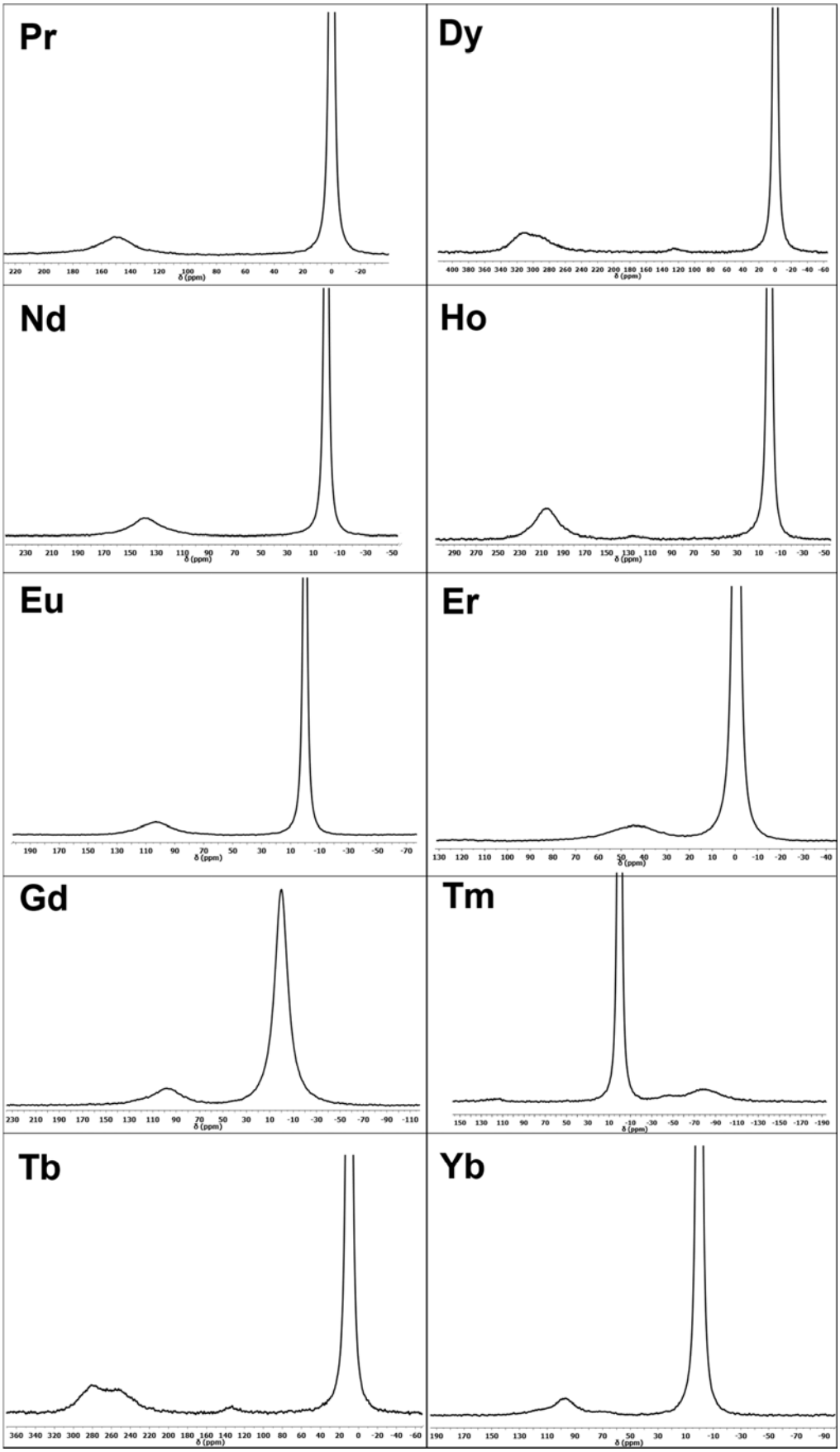

Figure S9. The ^{17}O NMR spectra of coordinated oxygen atom signals of some paramagnetic $[Ln(do3ap^{Me})]^{-}$.

The spectra were measured in D_2O (pD ~6.5, t = 5 °C, $\nu(^{17}O)$ = 81 MHz). The diastereoisomers were assigned by comparing relative integral intensities with ^{1}H NMR.

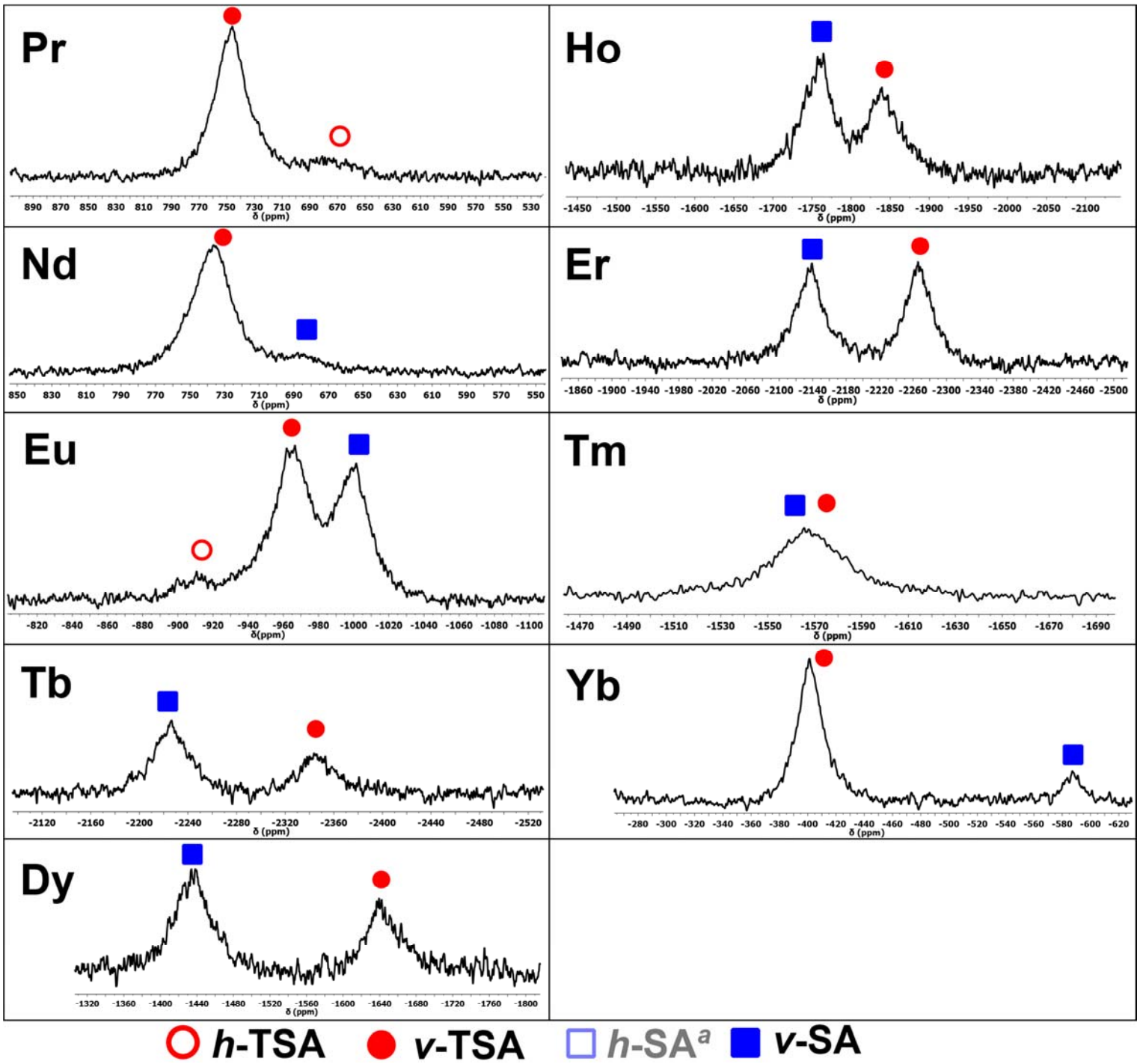

[a]The *h*-SA diastereoisomer's signals could not be assigned due to their low abundance.

^{13}C NMR relaxation times

Table S2. Relaxation rates R_1, R_2* and the corresponding dipolar contributions R_{1DD}, and rotational correlation times τ_R for some signals of [Lu(do3ap^{Me})]$^-$. Values are measured in D_2O (pD ~6.5, t = 5 °C, ν(^{13}C) = 151 MHz).

δ [ppm]	NOE factor	R_1 [s^{-1}]	R_2* [s^{-1}]	R_{1DD} [s^{-1}]	τ_R [ps]
15.5	–[a]	1.3	14.1[b]	–[a]	–[a]
48.0	2.3	5.1	–[a]	5.9	137
48.3	2.3	5.1	–[a]	5.9	138
48.4	2.1	5.6	–[a]	5.8	135
53.6	2.5	5.2	–[a]	6.6	153
53.7	2.3	5.3	–[a]	6.2	144
53.8	2.2	5.2	–[a]	5.7	133
54.0	2.3	5.2	–[a]	6.0	139
59.5	2.3	5.0	–[a]	5.8	135
59.6	2.3	5.0	–[a]	5.7	133
59.9	2.3	5.2	–[a]	5.9	137
179.6	–[a]	0.48	10.4	–[a]	–[a]
180.0	–[a]	0.46	10.4	–[a]	–[a]
180.2	–[a]	0.43	10.4	–[a]	–[a]

[a]Not determined. [b]Value for R_1 determined by CPMG as R_2* is not easily defined for multiplets.

For the assignment of some ^{13}C NMR signals of the [Yb(do3ap^{Me})]$^-$ complex, see **Figures S10** and **S11**. Signals of the carboxylate C=O groups were assigned from the ^{13}C NMR spectrum without ^{1}H decoupling as the only three singlets (**Figure S10**). Furthermore, they were assigned to the particular C=O groups based on their T_1 relaxation times increasing with the increasing Yb–C distance. The ^{13}C NMR signal of –CH_3 group was assigned from the ^{13}C NMR spectrum, selectively ^{1}H-decoupled at the frequency corresponding to –CH_3 ^{1}H NMR signal assigned based on its integral intensity (**Figure S11**). Only the signals of the major *v*-TSA diastereoisomer were assigned.

Figure S10. The ^{13}C NMR spectrum of [Yb(do3ap^{Me})]$^-$ in D_2O (pD ~6.5, t = 5 °C, ν(^{13}C) = 151 MHz) without ^{1}H decoupling with three singlets corresponding to the C=O groups.

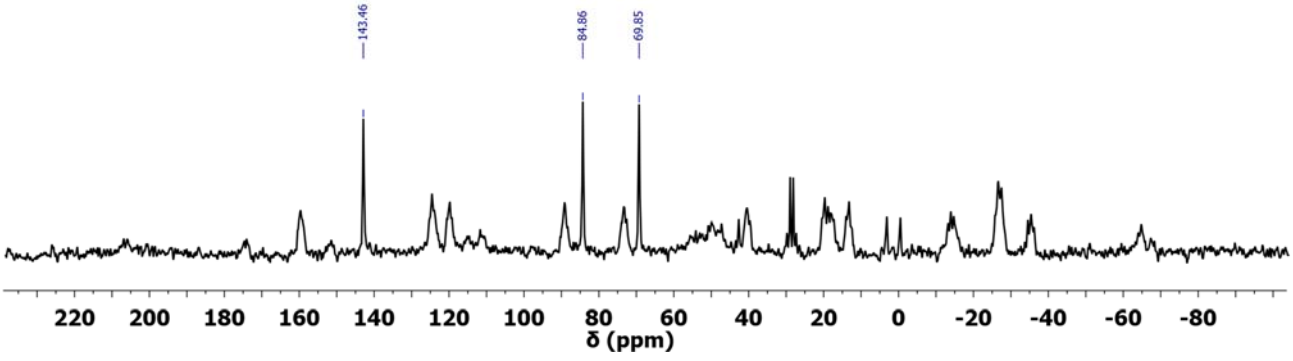

Figure S11. A part of the ^{13}C NMR spectrum of $[Yb(do3ap^{Me})]^-$ in D_2O (pD ~6.5, t = 5 °C, $\nu(^{13}C)$ = 151 MHz) (**a**) without decoupling and (**b**) with a selective ^1H decoupling at the $-CH_3$ frequency displaying the ^{13}C signals of the methyl group of the two major diastereoisomers at −14.5 (d, $^1J_{CP}$ = 93 Hz, *v*-SA) and −13.1 (d, $^1J_{CP}$ = 95 Hz, *v*-TSA).

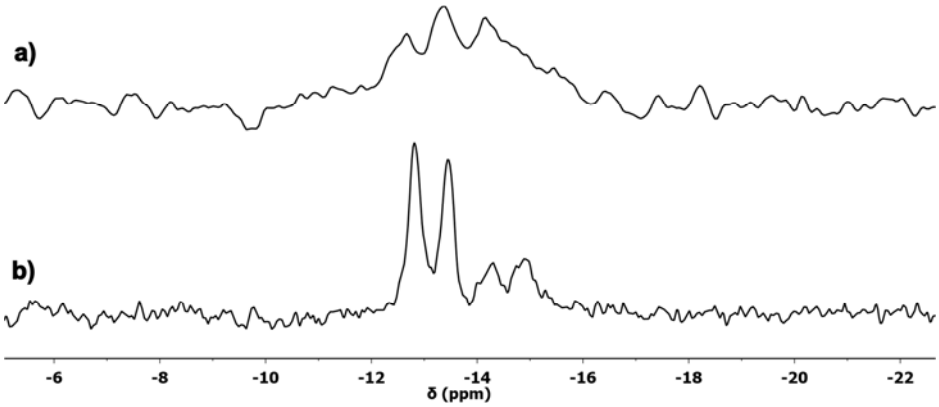

Table S3. Relaxation rates R_1 and R_2* ($\nu(^{13}C)$ = 151 MHz) and the calculated Yb–C distances for selected ^{13}C atoms of the $[Yb(do3ap^{Me})]^-$ complex.

Values are at 0 °C and 5 °C, and Yb–C distances were calculated by the Equation (1) in the main text from the difference of the paramagnetical contributions to R_1 and R_2* at 5 °C. Values of relaxation times at 0 °C were only used to determine the ratio of distances Yb···C=O and Yb···CH_3 from the ratio of the paramagnetic contributions to the R_1 relaxation times, the Equation (2) in the main text.

δ_C [ppm]	Atom type	R_1 (0 °C) [s^{-1}]	R_1 (5 °C) [s^{-1}]	R_2* (5 °C) [s^{-1}]	r [Å]
179.6	C=O	72.9	71.8	89.5	3.0
180.0	C=O	63.4	58.7	75.4	3.1
180.2	C=O	64.7	60.9	78.5	3.0
5.5	H_3C–P	9.88	8.62	22.6	4.2

DFT Calculations

Table S4. DFT-calculated relative free energies E_{rel} (kJ mol^{-1}).

Free energies of all diastereoisomers and transition states for both the experimentally confirmed h-TSA/v-TSA and hypothetical *h*-SA/*v*-SA phosphinate rotation of the [Ln(do3ap^{Me})(H$_2$O)]$^-$ complexes (Ln = La–Eu) were calculated by DFT (relative to the most stable diastereoisomer; in bold) with one coordinated water molecule. Energies of diastereoisomers and transition states of the [La/Eu(do3ap^{OEt})]$^-$ complexes calculated by the same method are included for comparison. Furthermore, free energies of *h*-TSA' and v-TSA' diastereoisomers of [Yb(do3ap^{Me})]$^-$ without a coordinated water molecule and a corresponding transition state for hypothetical *h*-TSA′/v-TSA′ phosphinate rotation were calculated analogously and are included. Moreover, Gibbs energies of activation for phosphinate rotation calculated from these values and weighted by diastereoisomer abundances, are shown. Diastereoisomers are defined as follows: *v*-SA = *S*-Δλλλλ/*R*-Λδδδδ, *h*-SA = *R*-Δλλλλ/*S*-Λδδδδ, *v*-TSA = *R*-Λλλλλ/*S*-Δδδδδ and *h*-TSA = *S*-Λλλλλ/*R*-Δδδδδ.

Ln^{III}	[Ln(do3ap^{Me})(H$_2$O)]$^-$							
	h-SA	*v*-SA	*SA TS*[a]	*h*-TSA	**v-TSA**	TSA TS	$^{298}\Delta G^{\ddagger}$ *(SA)*[a]	$^{298}\Delta G^{\ddagger}$ (TSA)
La	20.9	11.7	*58.4*	4.7	**0.0**	33.3	*37.8*	28.8
Ce	19.0	10.6	*59.9*	4.4	**0.0**	36.1	*41.2*	31.9
Pr	17.9	9.6	*63.2*	4.3	**0.0**	41.4	*45.8*	37.4
Nd	17.3	9.5	*66.8*	4.3	**0.0**	46.8	*49.7*	42.7
Sm	14.4	6.6	*72.5*	4.2	**0.0**	53.6	*58.3*	49.6
Eu	12.9	5.1	*75.4*	3.5	**0.0**	56.2	*62.7*	52.9
Yb[b]	–	–	–	4.5[c]	**0**[c]	112.1[a]	–	107.8[a]
	[Ln(do3ap^{OEt})(H$_2$O)]$^-$							
La	12.9	11.6	*60.8*	1.3	**0**	36.1	*47.1*	36.0
Eu	7.0	7.4	*79.0*	**0**	1.2	60.8	*72.1*	59.7

[a]Hypothetical dynamic process

[b]Complex with no coordinated water molecule.

[c]Calculated for diastereoisomers TSA′.

Figure S12. DFT-calculated structures.

An example of the DFT-calculated structures of diastereoisomers *v*/*h*-SA, and *v*/*h*-TSA for the $[La(do3ap^{Me})(H_2O)]^-$ and *v*/*h*-TSA′ for $[Yb(do3ap^{Me})]^-$ complexes and of the "phosphinate rotation" transition states. Visualized in VESTA[2]. Hydrogen atoms (with the exception of CH_3) are not shown for clarity. Colour code: **hydrogen – white**, **carbon – grey**, **nitrogen – blue**, **oxygen – red**, **phosphorus – orange** and **lanthanide – green**.

$[La(do3ap^{Me})(H_2O)]^-$

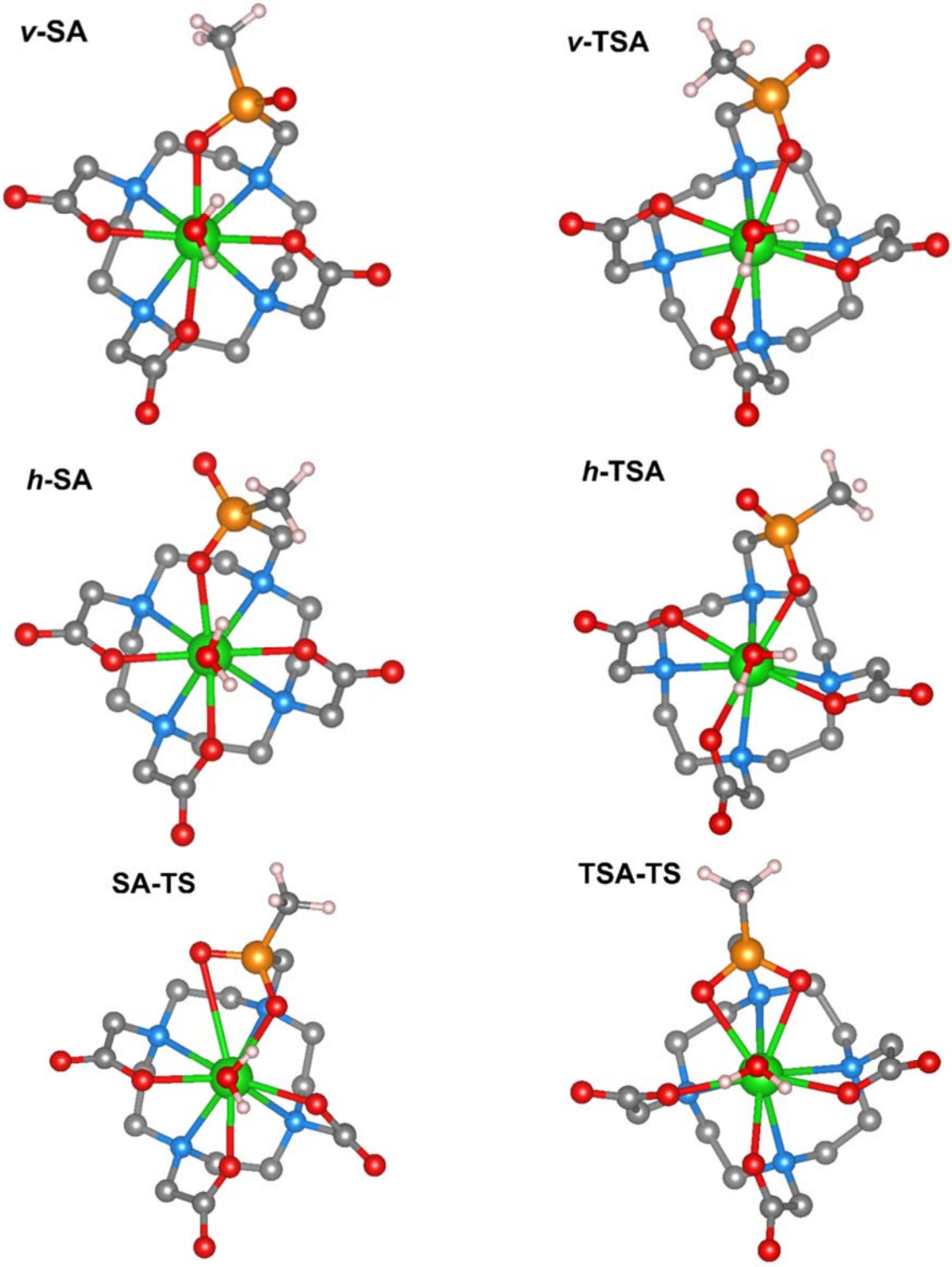

[Yb(do3ap^{Me})]$^{-}$

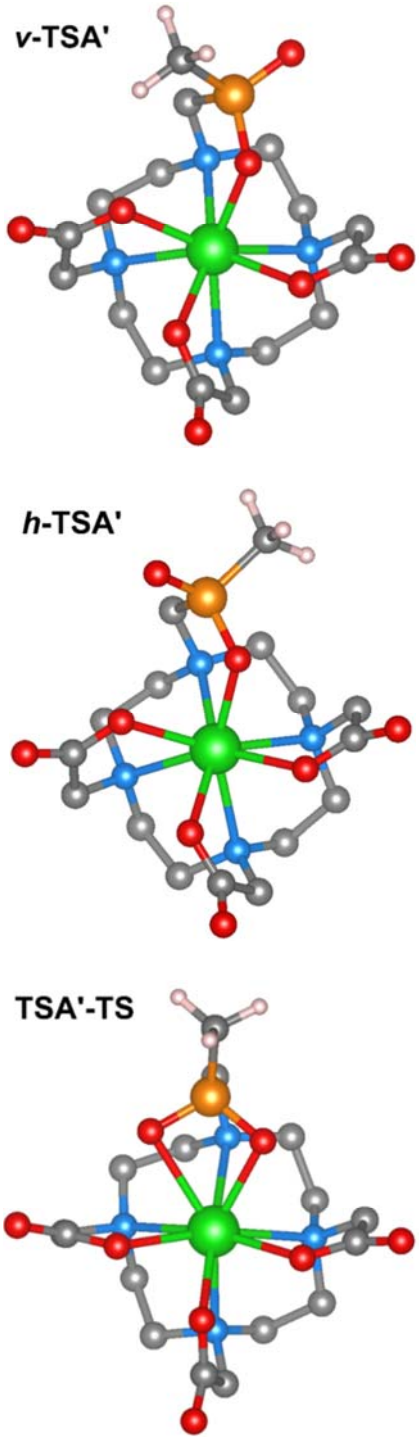

Diastereoisomer abundances

Figure S13. Abundances of the SA, TSA and TSA′ isomers for the [Ln(do3ap^{Me})]$^{-}$ complexes. The abundances were determined at 5 °C from integral intensities obtained from the ^{1}H and ^{31}P NMR spectra.

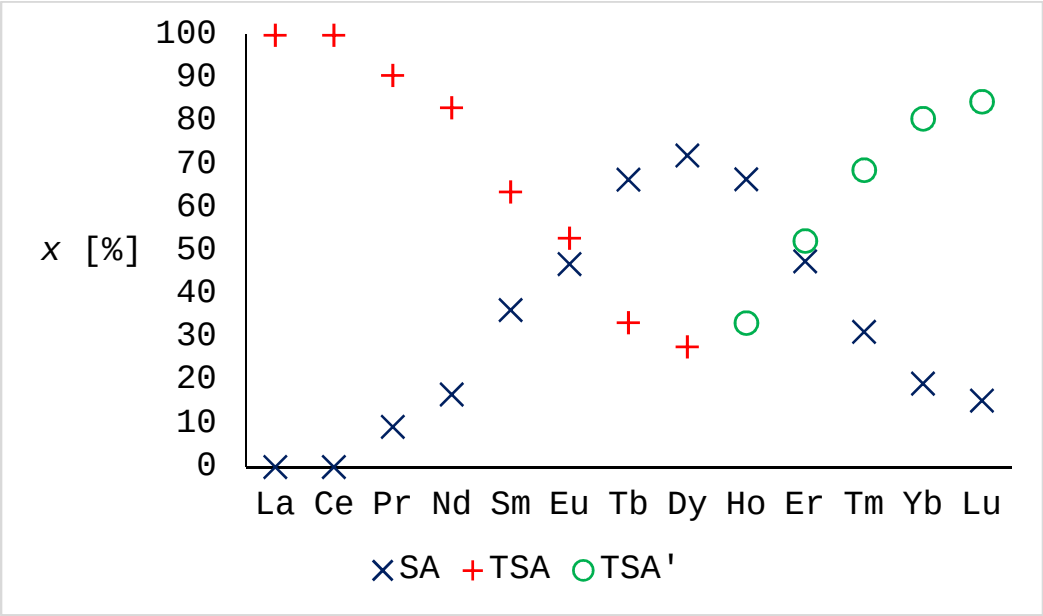

Figure S14. Dependence of TSA/SA ratio on temperature for some [Ln(do3ap^{Me})]$^{-}$ complexes.

Data are based on relative integral intensities of ^{31}P NMR signals of some [Ln(do3ap^{Me})]$^{-}$ complexes at temperatures with a sufficient resolution of the ^{31}P NMR signals.

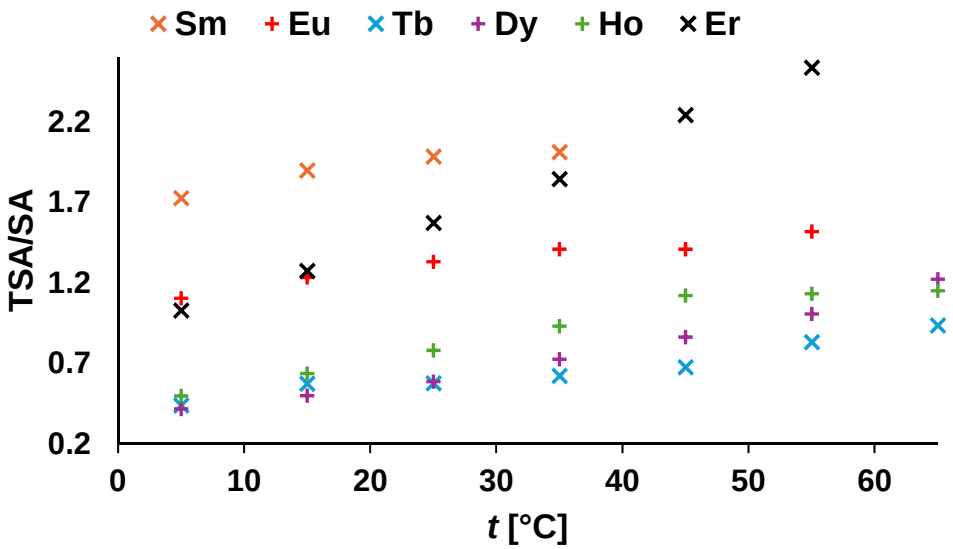

Table S5. Relative ratios of *vertical*-to-*horizontal* diastereoisomer abundances for selected [Ln(do3ap^{Me})]$^-$ at multiple temperatures.

The ratios were determined from relative integral intensities of ^{31}P NMR signals and represent the percentage of the corresponding *vertical* isomers in relation to the sum of *vertical* and *horizontal* isomers of the same type (SA or TSA).

t [°C]	Eu		Dy		Er		Yb	
	v-TSA (%)	*v*-SA (%)	*v*-TSA (%)	*v*-SA (%)	*v*-TSA (%)	*v*-SA (%)	*v*-TSA (%)	*v*-SA (%)
5	92	96	95	95	95	98	96	–[a]
15	91	96	95	97	96	98	95	–[a]
25	91	97	95	96	94	97	96	–[a]
35	92	–[a]	94	98	94	99	95	–[a]
45	–[a]	–[a]	95	95	95	–[a]	–[a]	–[a]
55	–[a]	–[a]	–[a]	–[a]	95	–[a]	–[a]	–[a]

[a] Signals were not resolved.

Table S6. Relative ratios of *vertical*-to-*horizontal* diastereoisomer abundances for selected [Ln(do3ap^{Me})]$^-$ complexes.

Abundances are based on relative integral intensities of ^{31}P NMR signals (average from all measured temperatures with resolved signals). The percentages shown were determined with respect to the sum of *v*-TSA and *h*-TSA or *v*-SA and *h*-SA.

Isomer	Sm	Eu	Tb	Dy	Er	Yb
v-TSA (%)	89	91	96	95	95	95
v-SA (%)	96	97	96	96	98	–

NMR study of the [Eu(do3ap^{Me})(H_2O)]$^-$ complex

Figure S15. An example of a 2D ^{1}H–^{1}H EXSY spectrum of the [Eu(do3ap^{Me})(H_2O)]$^-$ complex.

Spectrum was measured at t = 5 °C (D_2O, pD ~6.5, ν(^{1}H) = 600 MHz) and τ_m = 15 ms, and shows cross-peaks of different processes. Dynamic processes: **blue – macrocycle inversion**, **red – pendant arms re-orientation**, **green – phosphinate rotation** and **purple – combination of macrocycle inversion and pendant arms re-orientation**.

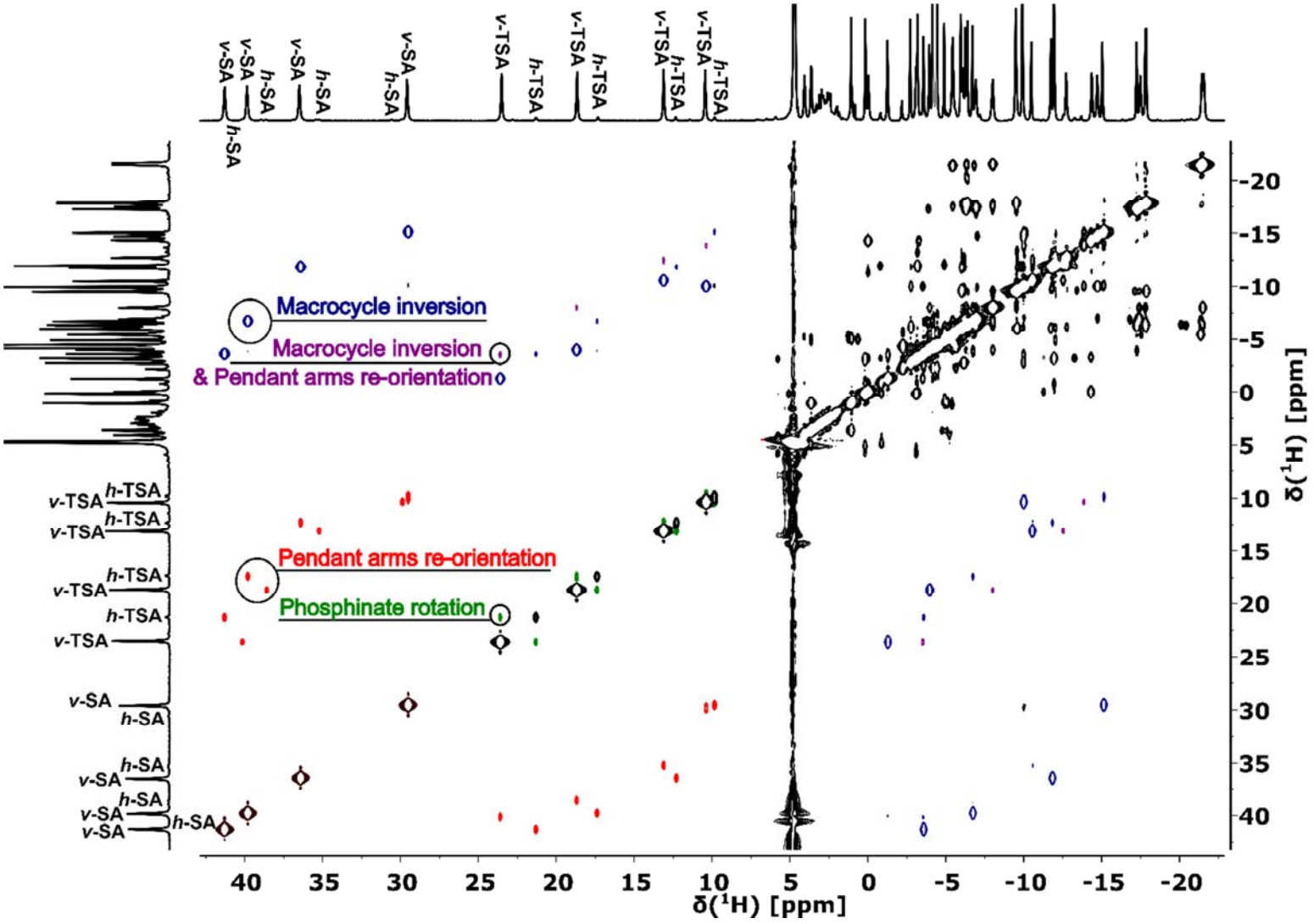

Figure S16. The ^{1}H–^{1}H COSY spectrum of the [Eu(do3ap^{Me})(H_2O)]$^{-}$ complex at t = 5 °C (D_2O, pD ~6.5, ν(^{1}H) = 600 MHz). Spectrum was used to assign some of the ^{1}H NMR signals.

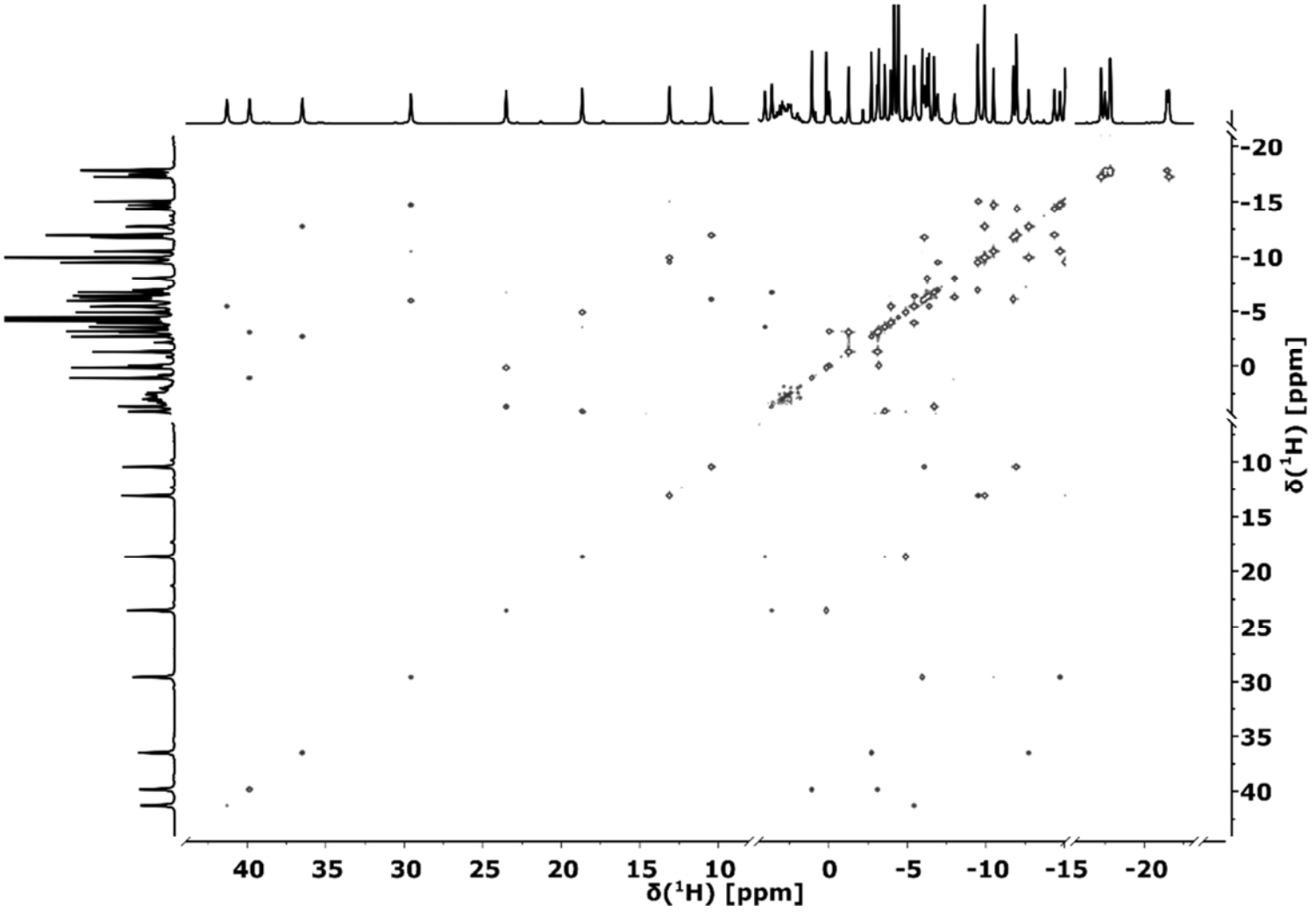

Figure S17. An example of 2D ^{31}P–^{31}P EXSY spectrum of the [Eu(do3ap^{Me})(H$_2$O)]$^-$ complex at t = 5 °C (D$_2$O, pD ~6.5, ν(^{31}P) = 243 MHz) and τ_m = 15 ms. The spectrum was used for the quantitative determination of rates of the dynamic processes.

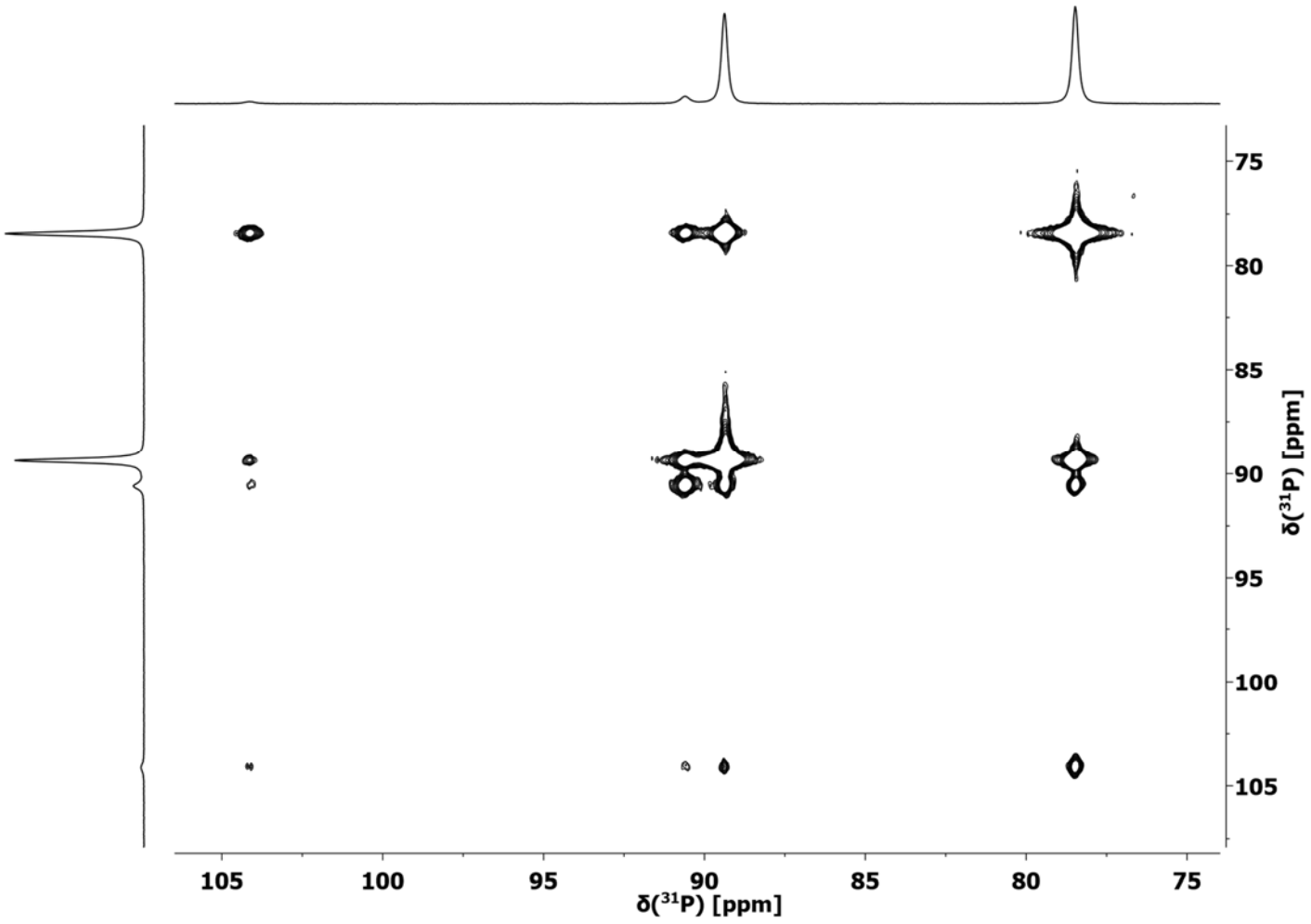

Table S7. Rate constants k_{ex} and relaxation rates R_1 calculated from the ^{31}P–^{31}P EXSY of the [Eu(do3ap^{Me})(H$_2$O)]$^-$ complex.

Values are in the form of mean ± standard deviation (based on values determined at multiple τ_m). Values of the rate constants are defined for a process in the direction **X** (shown in row header) → Y (shown in column header). For **X** = *Y*, the values shown are the R_1. The small values of rate constants for the hypothetical *v*-SA/*h*-SA exchange likely only result from the experimental error resulting from the method and model used, as this process does not take place according to the 2D ^{1}H–^{1}H EXSY.

k_{ex} [s^{-1}] or R_1 [s^{-1}]				
X→*Y*	*h-SA*	*h-TSA*	*v-SA*	*v-TSA*
***h*-SA**	34±11	31±4	8±3	107±5
***h*-TSA**	11.5±1.5	55±28	10±6	15±1
***v*-SA**	0.33±0.12	1.0±0.6	26.5±1.1	14.3±0.2
***v*-TSA**	3.9±0.2	1.45±0.08	13.2±0.2	25.8±0.6

Table S8. Comparison of equilibrium constants.

Constants were calculated from ^{31}P–^{31}P EXSY rate constants, *K*(EXSY), and from ^{31}P NMR integral intensities, *K*(int), at 5 °C (D_2O, pD ~6.5, ν(^{31}P) = 243 MHz) for the equilibria **X (shown in row header)** ⇌ *Y(shown in column header)*.

Isomer	*K*(EXSY), **X** ⇌ *Y*				*K*(int), **X** ⇌ *Y*			
	h-SA	*h-TSA*	*v-SA*	*v-TSA*	*h-SA*	*h-TSA*	*v-SA*	*v-TSA*
***h*-SA**	–	0.38	0.04	0.04	–	0.41	0.04	0.04
***h*-TSA**	2.66	–	0.10	0.10	2.45	–	0.10	0.09
***v*-SA**	25.5	9.59	–	0.92	23.7	9.7	–	0.92
***v*-TSA**	27.8	10.4	1.09	–	25.8	10.5	1.09	–

Variable-temperature ^{17}O NMR

Figure S18. The ^{17}O NMR spectra (D_2O, pD ~6.5, $\nu(^{17}O)$ = 81 MHz) of complexes where phosphinate rotation was detected at various temperatures.

For H_4do3ap^{Me} complexes of Ln = La–Sm, the spectra are shown along with the fit (in red) to Equation (S4), see ESI Experimental, used to determine the activation parameters.

[La(do3ap^{Me})(H_2O)]$^-$

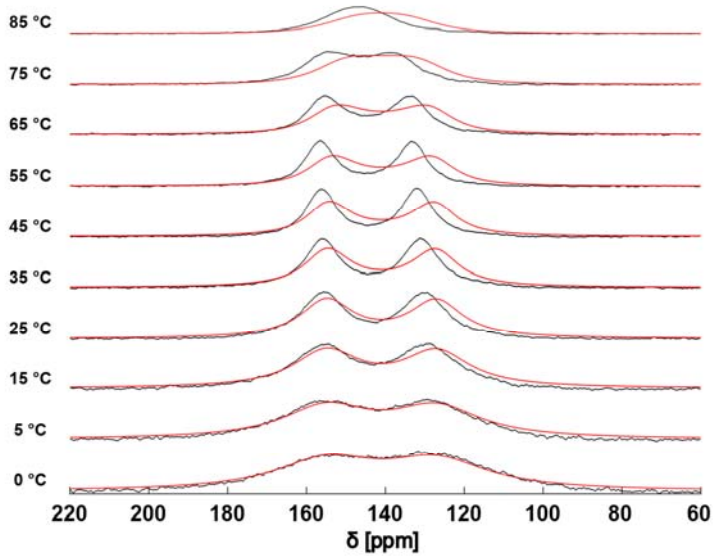

[Ce(do3ap^{Me})(H_2O)]$^-$

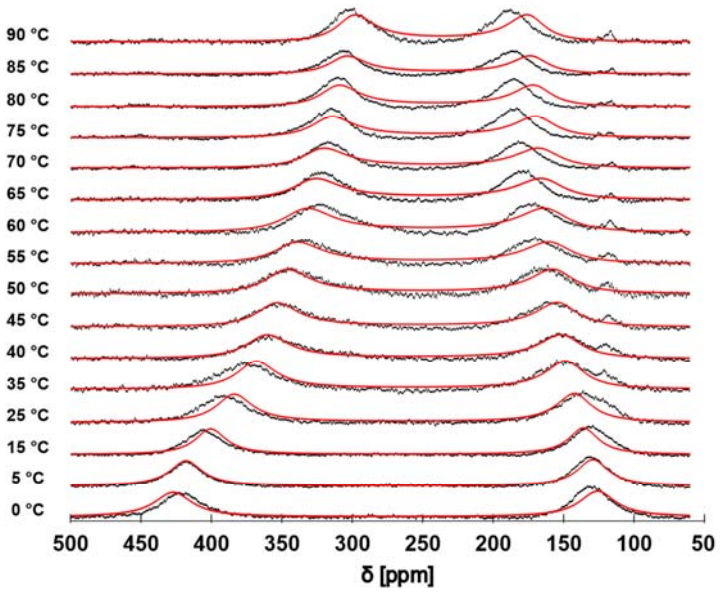

[Pr(do3ap^{Me})(H_2O)]$^-$

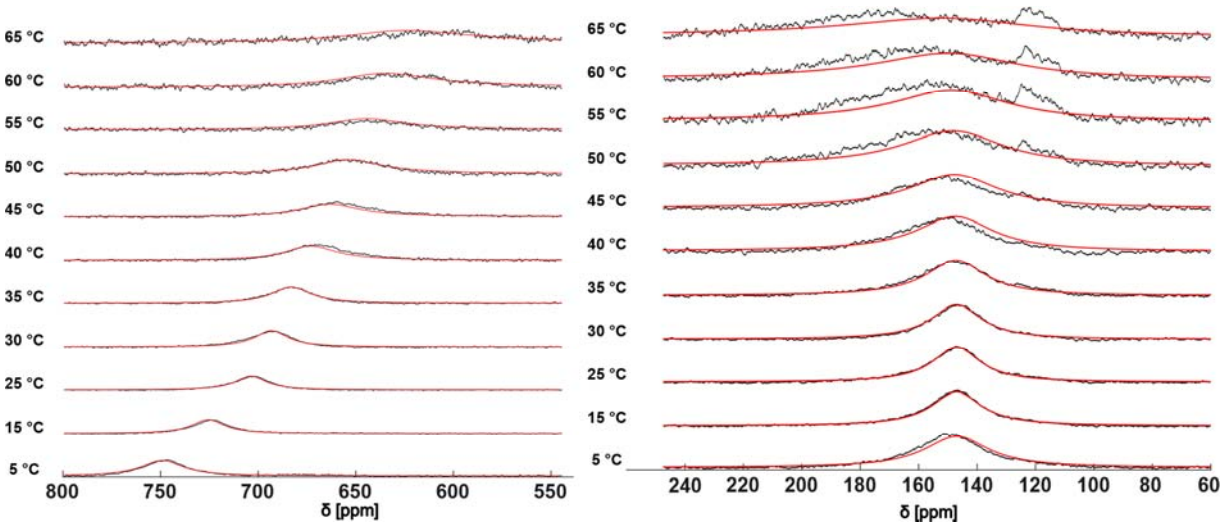

[Nd(do3ap^{Me})(H_2O)]$^-$

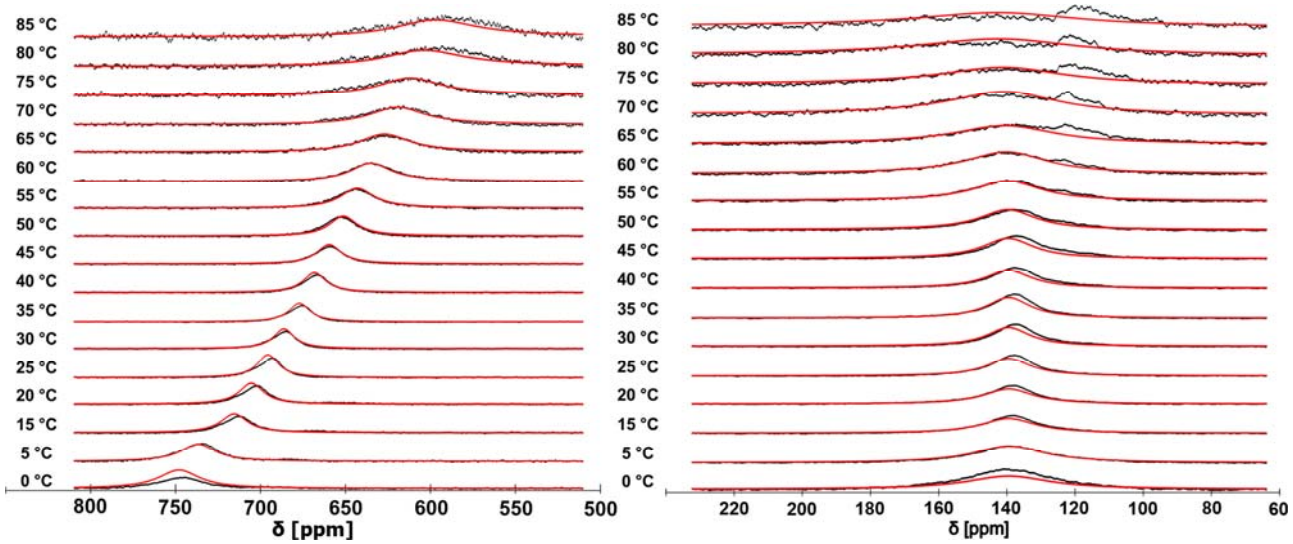

[Sm(do3ap^{Me})(H_2O)]$^-$

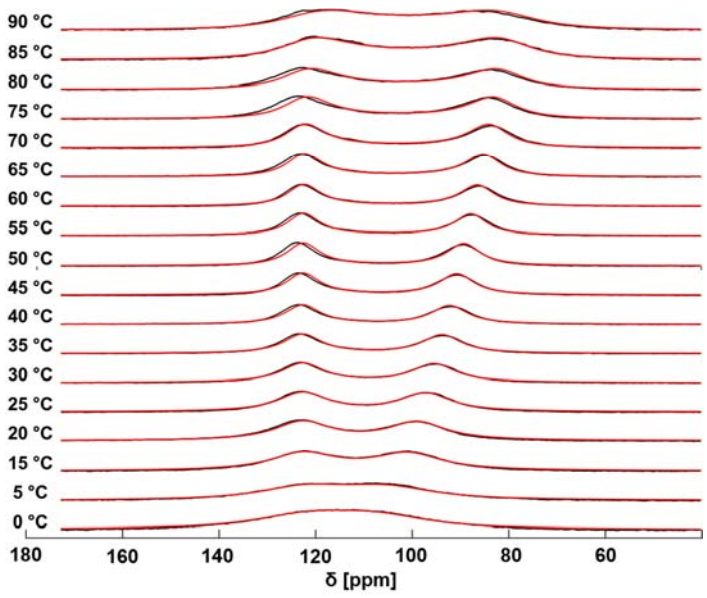

$[Eu(do3ap^{Me})(H_2O)]^-$

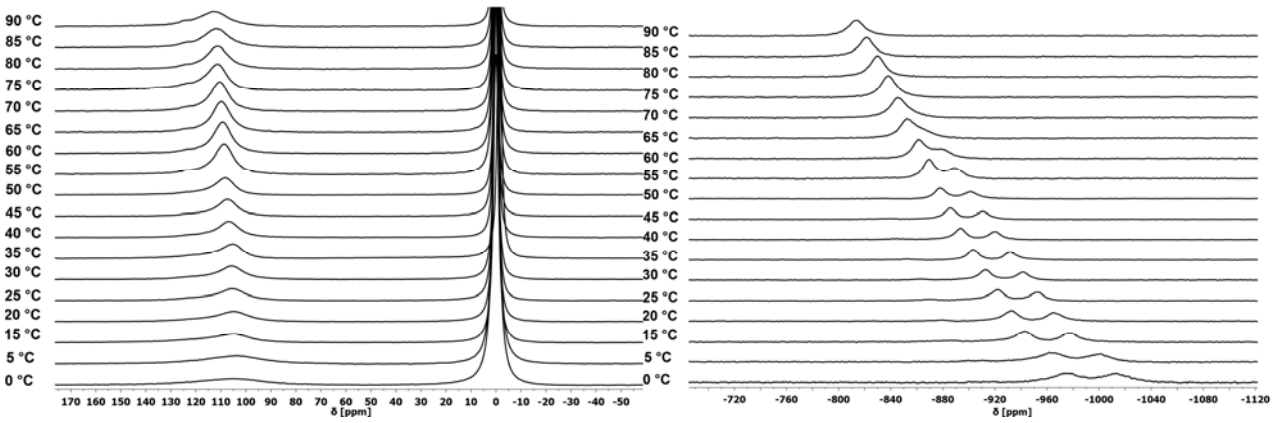

Figure S19. The ^{17}O NMR spectra of complexes without phosphinate rotation.

$[Gd(do3ap^{Me})(H_2O)]^-$

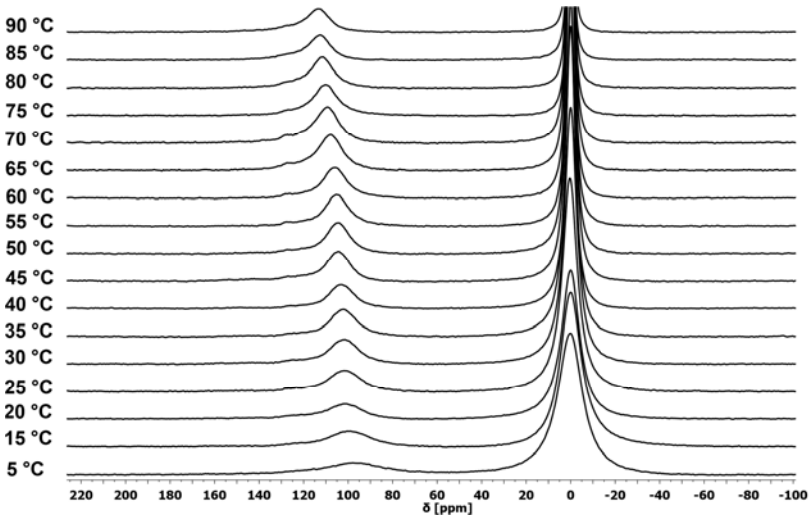

$[Tb(do3ap^{Me})(H_2O)]^-$

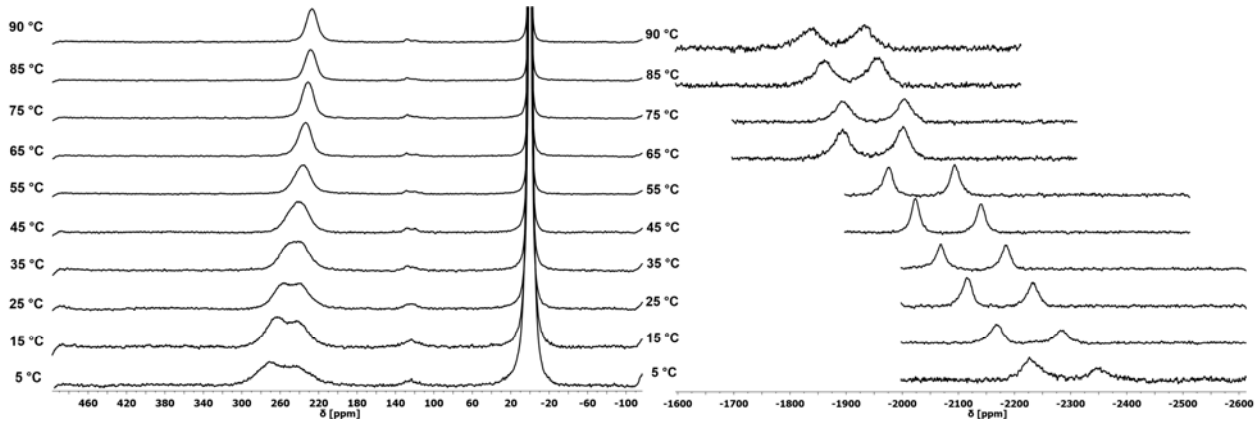

$[Dy(do3ap^{Me})(H_2O)_{0-1}]^-$

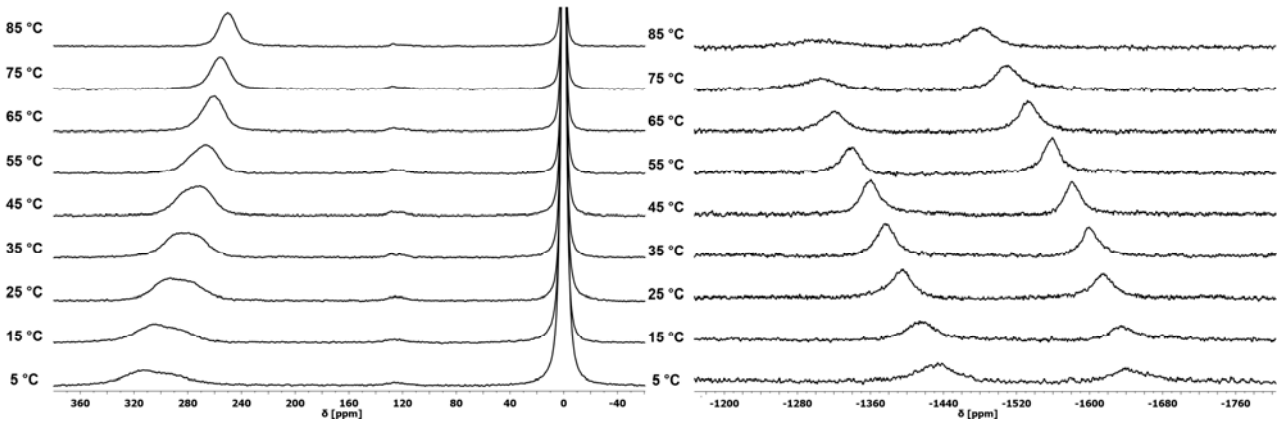

$[Ho(do3ap^{Me})(H_2O)_{0-1}]^-$

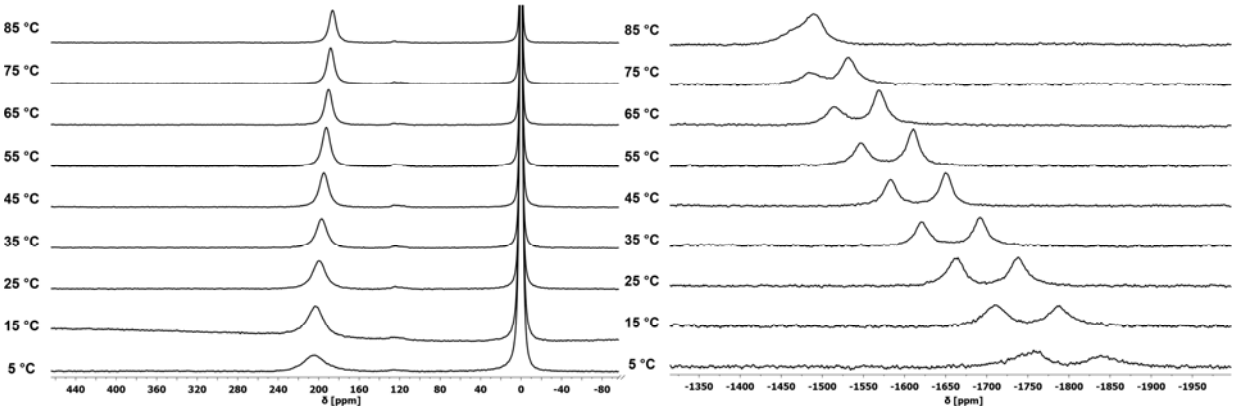

$[Er(do3ap^{Me})]^-$

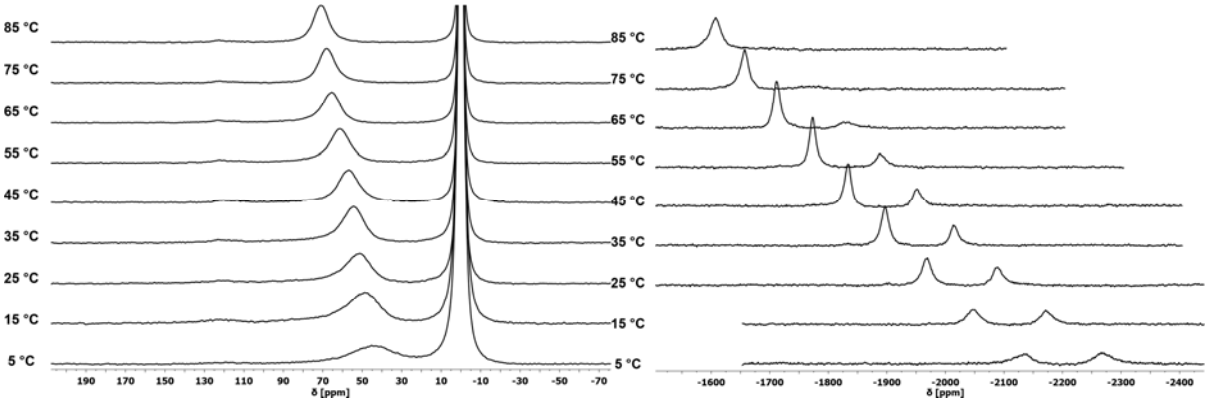

$[Yb(do3ap^{Me})]^-$

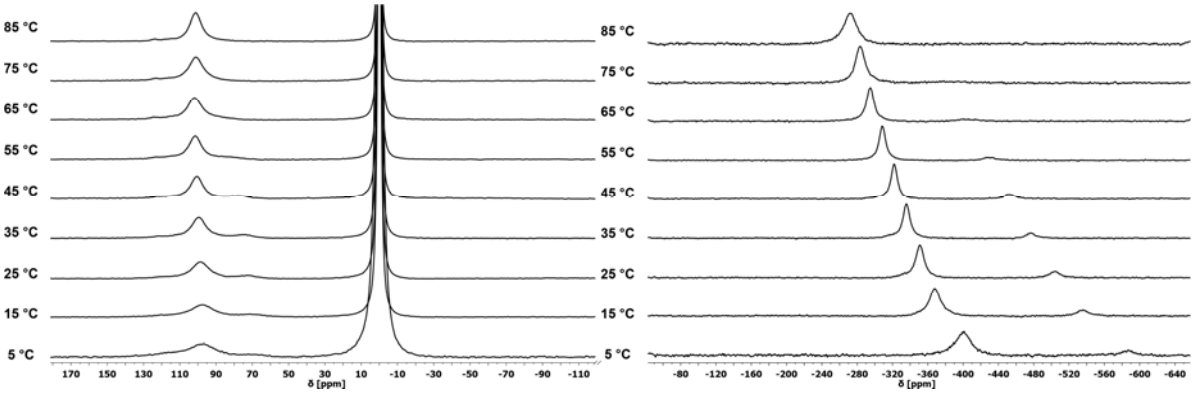

$[Lu(do3ap^{Me})]^-$

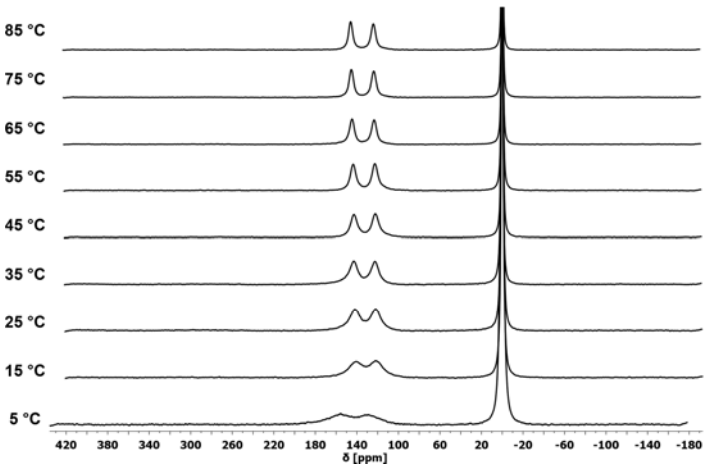

Table S9. Experimental rate constants, k_{ex}, of the phosphinate rotation.

Rate constants were determined in some $[Ln(do3ap^{Me})]^-$ complexes by fitting the VT ^{17}O NMR to Equation (S4); for detail, see the Experimental part.

t [°C]	k_{ex} ($[Ln(do3ap^{Me})]^-$) [s^{-1}]				
	La	Ce	Pr	Nd	Sm
15	–[a]	$(1.26\pm0.25)\cdot10^3$	$(2\pm4)\cdot10^3$	–[a]	–[a]
20	–[b]	–[b]	–[b]	$(2\pm5)\ \ 10^2$	–[a]
25	–[a]	$(4.69\pm0.25)\cdot10^3$	$(1.2\pm0.4)\cdot10^3$	$(2\pm5)\ \ 10^2$	–[a]
30	–[b]	–[b]	$(1.9\pm0.5)\cdot10^3$	$(6\pm5)\ \ 10^2$	–[a]
35	$(6\pm7)\cdot10^2$	$(9.5\pm0.4)\cdot10^3$	$(3.3\pm0.6)\cdot10^3$	$(1.0\pm0.5)\ \ 10^3$	–[a]
40	–[b]	$(1.43\pm0.06)\cdot10^4$	$(5.4\pm1.2)\cdot10^3$	$(1.6\pm0.5)\cdot10^3$	$(1\pm3)\cdot10^2$
45	$(1.1\pm1.0)\cdot10^3$	$(1.63\pm0.09)\cdot10^4$	$(7.0\pm1.1)\cdot10^3$	$(2.3\pm0.4)\cdot10^3$	$(3\pm3)\cdot10^2$
50	–[b]	$(1.95\pm0.08)\cdot10^4$	$(8.5\pm0.5)\cdot10^3$	$(3.0\pm0.4)\cdot10^3$	$(4\pm3)\cdot10^2$
55	$(2.0\pm1.1)\cdot10^3$	$(2.30\pm0.11)\cdot10^4$	$(1.0\pm0.4)\cdot10^4$	$(4.4\pm0.3)\cdot10^3$	$(5\pm3)\cdot10^2$
60	–[b]	$(2.57\pm0.10)\cdot10^4$	$(1.3\pm0.4)\cdot10^4$	$(5.7\pm0.4)\cdot10^3$	$(8\pm3)\cdot10^2$
65	$(2.8\pm1.1)\cdot10^3$	$(2.80\pm0.14)\cdot10^4$	$(1.8\pm0.5)\cdot10^4$	$(7.8\pm0.6)\cdot10^3$	$(1.1\pm0.3)\cdot10^3$
70	–[b]	$(2.85\pm0.12)\cdot10^4$	–[a]	$(8.7\pm0.5)\cdot10^3$	$(1.5\pm0.3)\cdot10^3$
75	$(4.43\pm0.9)\cdot10^3$	$(2.90\pm0.12)\cdot10^4$	–[a]	$(1.00\pm0.05)\cdot10^4$	$(2.1\pm0.4)\cdot10^3$
80	–[b]	$(3.03\pm0.13)\cdot10^4$	–[a]	$(1.31\pm0.05)\cdot10^4$	$(2.9\pm0.4)\cdot10^3$
85	$(5.44\pm0.8)\cdot10^3$	$(3.10\pm0.11)\cdot10^4$	–[a]	$(1.36\pm0.07)\cdot10^4$	$(3.9\pm0.5)\cdot10^3$
90	–[b]	$(3.27\pm0.12)\cdot10^4$	–[b]	–[b]	$(5.3\pm0.7)\cdot10^3$

[a]Error larger than the calculated value. [b]Not measured.

Table S10. Experimental activation parameters $\Delta H^{\ddagger}$, $\Delta S^{\ddagger}$ and $^{298}\Delta G^{\ddagger}$ of phosphinate rotation in the $[Ln(do3ap^{Me})]^{-}$ complexes.

The activation parameters were calculated from rate constants determined by VT ^{17}O NMR spectra using the Eyring equation. The values for the La^{III} do not agree with the trend due to the high error in their determination, which is due to the poor resolution of ^{17}O NMR signals.

Ln^{III}	$[Ln(do3ap^{Me})]^{-}$		
	$\Delta H^{\ddagger}$ [kJ mol^{-1}]	$\Delta S^{\ddagger}$ [J K^{-1} s^{-1}]	$^{298}\Delta G^{\ddagger}$ [kJ mol^{-1}]
La	33.97	–79.65	57.7
Ce	24.5	–88.4	50.9
Pr	44.9	–31.6	54.3
Nd	37.8	–61.2	56
Sm	62.6	–3.06	63.5

Figure S20. The best fits of phosphinate rotation rate constants to the Eyring equation.

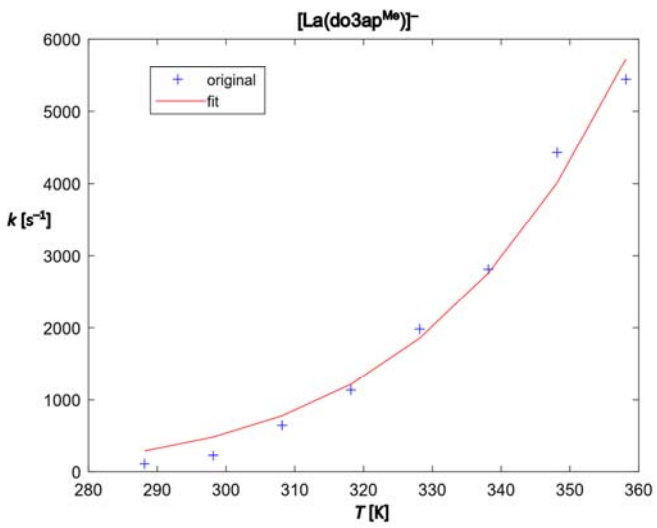

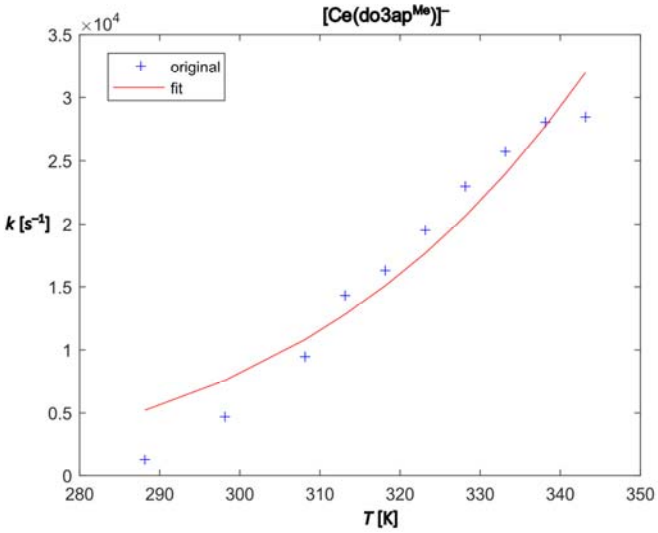

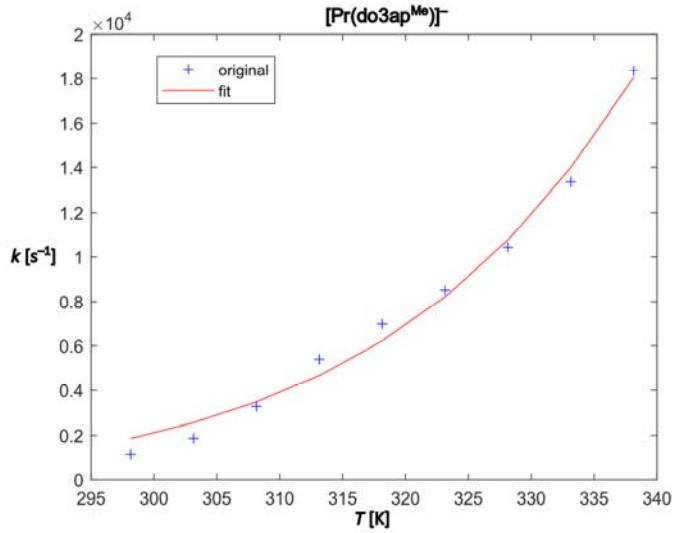

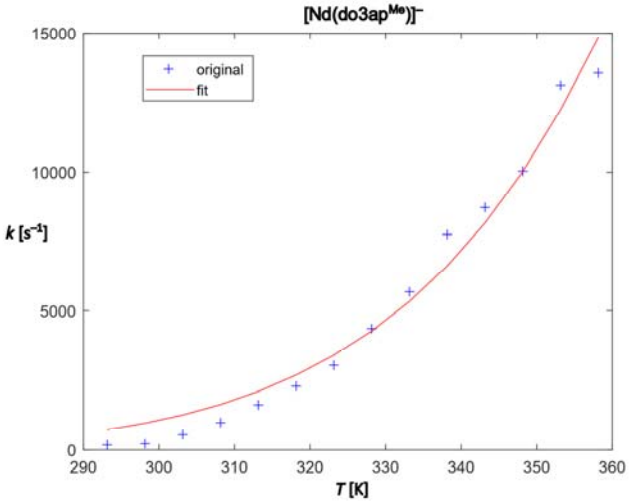

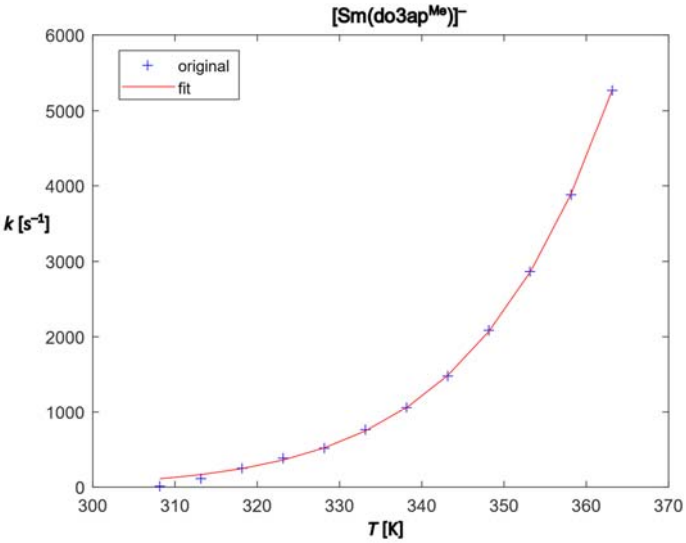

Figure S21. The DFT calculated structures of all four diastereoisomers of the $[Gd(H_2O)(do3ap^{Me})]^-$ complex with four water molecules in the second hydration sphere. Hydrogen bonds are shown as dashed lines. Hydrogen atoms bound to the macrocycle and pendant arm carbon atoms are not shown for clarity. Visualised in Vesta[2].

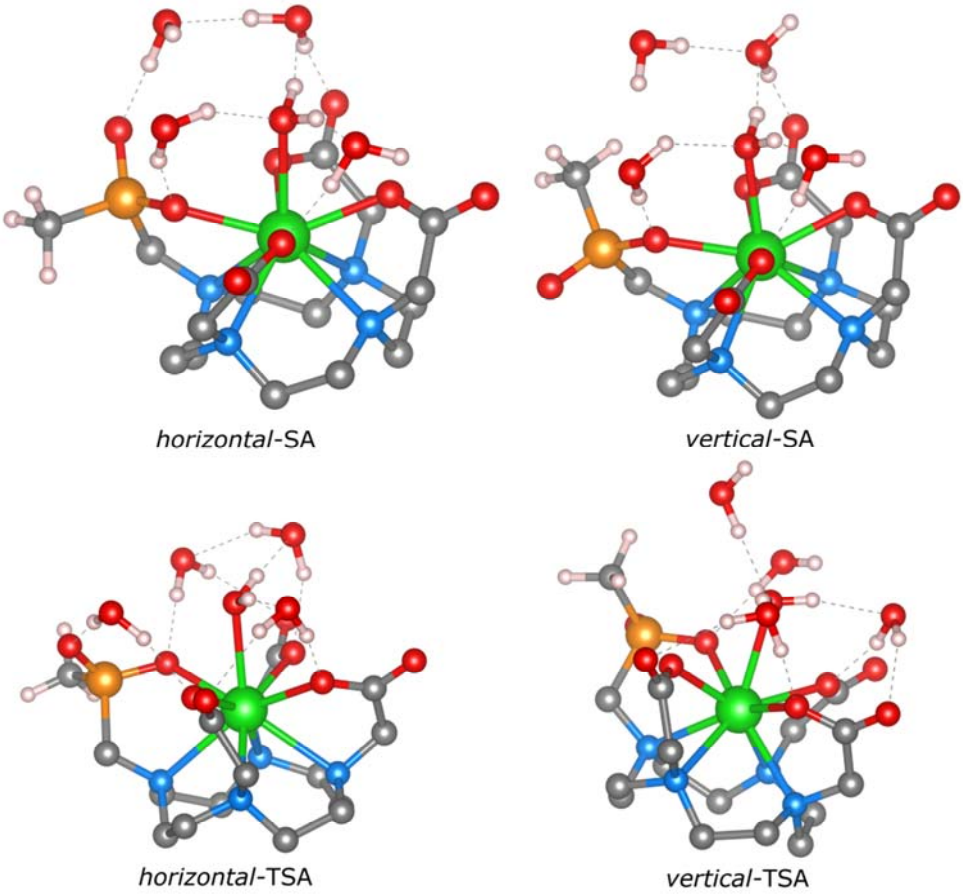

Table S11. Comparison of $^{298}\Delta G^{\ddagger}$ [kJ mol^{-1}] for dynamic processes.

Experimental (in bold, see also **Table S10**) or *DFT-calculated* (in italics) $^{298}\Delta G^{\ddagger}$ values of the phosphinate rotation in the *TSA*-[Ln(do3ap^{Me})]$^{-}$ complexes. Literature data for dynamic processes in the *TSA*-[Ln(do3ap^{OEt})]$^{-}$ and the [Ln(dota)]$^{-}$ complexes are added for comparison.

Ln	$^{298}\Delta G^{\ddagger}$ [kJ mol^{-1}]				
	[Ln(do3ap^{Me})]$^{-}$	[Ln(do3ap^{OEt})]$^{-}$ [1]	[Ln(dota)]$^{-}$ [3]–[13]		
	Phosphinate rotation	Phosphonate rotation	SA→TSA or SA→TSA′	TSA racemization	Carboxylate rotation
La	**57.7**, *48*	**51.8**, *52*	–[a]	60.7	74
Ce	**50.9**, *49*	**52.8**, *56*	–[a]	–[b]	–[b]
Pr	**54.3**, *52*	**55.7**, *58*	54	–[b]	77.5
Nd	**56**, *54*	**57.1**, *61*	–[b]	–[b]	90
Sm	**63**, *58*	**64**, *69*	–[b]	–[b]	94
Eu	*60*	**61**, *72*	64 (62)[c], *60* 62.7 (64)[c], *62*	–[b]	–[b]
Dy	–[a]	–[a]	68	–[b]	–[b]
Ho	–[a]	–[a]	65	–[b]	–[b]
Tm	–[a]	–[a]	65	–[b]	–[b]
Yb	*104*	–[a]	65.7	–[b]	–[b]
Lu	–[a]	–[a]	62.7	–[b]	136

[a]The process does not occur. [b]Value is not reported. [c]The assignment of the values to the processes differs in the literature[5],[6].

Experimental details

Materials and Methods

Methyl-dichlorophosphine, cyclen (1,4,7,10-tetraazacyclododecane), hydrated Ln^{III} chlorides, other reagents and solvents (including anhydrous THF and pyridine) were obtained from commercial sources and were used without further purification. The $H_2{}^{17}O$ (approx. 12% ^{17}O) was prepared by diluting a commercial $H_2{}^{17}O$ (approx. 60 % ^{17}O, CIL) with deionised water. The *t*Bu$_3$do3a·HBr (*t*Bu$_3$do3a = 1,4,7-tris(*t*-butoxycarbonylmethyl)-1,4,7,10-tetraazacyclododecane) was prepared from cyclen by a published procedure.[14]

The NMR spectra for characterisation of the synthesised compounds were measured on a Varian VNMRS 300 (300 and 121 MHz for ^1H and ^{31}P, respectively) and a Bruker Avance III 400 (400, 162, 101 and 54 MHz for ^1H, ^{31}P, ^{13}C and ^{17}O, respectively). The ^1H and $^{31}C\{^1H\}$ NMR spectra were referenced to the $–CH_3$ chemical shift of tetramethylsilane or *t*BuOH for solutions in $CDCl_3$ and D_2O, respectively. The ^{31}P NMR spectra were referenced to the chemical shift of the 85% aq. H_3PO_4 in an external capillary tube, and the ^{17}O NMR spectra to the external 1% $H_2{}^{17}O$ in D_2O or the solvent $D_2{}^{17}O$ signal for the spectra measured in $CDCl_3$ and D_2O, respectively. The pD values are the corrected pH values determined by a pH electrode calibrated to the standard buffer solutions, pD = pH + 0.4. Where necessary, the pD of NMR samples was increased by CsOD (ligands), LiOD (complexes) or DCl in D_2O. Concentrations of the paramagnetic complexes in the solutions were determined by the Evans method (Table S13 and the accompanying text). The NMR sample temperature was calibrated from the chemical shift difference of signals of pure CD_3OD (0–40 °C) or 80% (*w*/*w*) ethylene glycol in $(CD_3)_2SO$ (45–90 °C). Thin-layer chromatography (TLC) was carried out on TLC Silica Gel 60 F_{254} plates (Merck). Compounds with a P–H bond were visualised by 5% aq. $KMnO_4/K_2CO_3$/NaOH 12:80:1 mixture. The remaining compounds were visualised by applying I_2 vapours for 15 min. Mass spectra (MS) were measured on a Waters ACQUITY QDA spectrometer with a quadrupolar detection and an electrospray ionisation (positive or negative). The MS data were processed in the Empower 3 software. Elemental analyses of compounds were carried out at the IOCB (Prague, Czechia). The C/H/N content was determined by combustion analysis with a 2400 Series II Elemental Analyzer (Perkin Elmer) and P content was determined by an X-ray fluorescence analysis with an XEPOS P spectrometer (Spectro).

Variable-temperature ^1H, ^{31}P and ^{17}O NMR spectra of the $[Ln(do3ap^{Me})]^-$ complexes were measured on a Bruker Avance III 600 spectrometer equipped with a broadband probe by a pulse-acquire (^1H,^{31}P) or RIDE (^{17}O) pulse sequence. The experimental parameters (relaxation delays and acquisition times) were shortened due to the paramagnetic and quadrupolar relaxations (Table S12), and the number of transients was chosen to reach an acceptable signal-to-noise ratio. Spectra were measured at 0–90 °C with 5 °C or 10 °C steps. Before each measurement, every sample was kept at the desired temperature for 15 min to reach thermal equilibrium.

Table S12. Experimental relaxation delays d_1 and acquisition times t_a for measuring the NMR spectra of the $[Ln(do3ap^{Me})]^-$ complexes.

$[Ln(do3ap^{Me})]^-$	^{1}H NMR		^{31}P NMR		^{17}O NMR	
	d_1, s	t_a, s	d_1, s	t_a, s	d_1, s	t_a, s
La^{III}, Lu^{III}	5.0	3.4	3.0	0.3	0.1	0.08
Ce^{III}, Pr^{III}, Nd^{III}, Gd^{III} [a]	0.2	0.15	0.2	0.15	0.07	0.04
Sm^{III}	0.3	1	0.1	0.3	0.07	0.04
Eu^{III}	0.3	1.2	0.1	0.4	0.08	0.03
Tb^{III}, Dy^{III}, Ho^{III}, Er^{III}, Tm^{III}, Yb^{III}	0.1	0.1	0.1	0.1	0.07	0.04

[a]The Gd^{III} complex was detectable only in ^{17}O NMR spectra.

The 2D ^{1}H–^{1}H and ^{31}P–^{31}P EXSY spectra of the Eu^{III} complex (due to its favourable paramagnetic properties) were measured on a Bruker Avance III 600 spectrometer with a cryoprobe or a broadband probe, respectively, by a standard Bruker phase-sensitive NOESY pulse sequence and processed in the MestReNova©. The relaxation delays (d_1 = 0.3 s and 0.4 s for ^{1}H–^{1}H and ^{31}P–^{31}P EXSY, respectively) were shortened, and the mixing times were selected (< 20 ms) to account for the paramagnetic relaxation. The 2D ^{31}P–^{31}P EXSY was used to determine the rate constants of the dynamic processes. For this purpose, the ^{31}P–^{31}P EXSY spectra were measured at 13 different mixing times in the range of 1–20 ms where all four diagonal peaks and all 12 cross-peaks were detected.

The T_1 of ^{13}C signals were determined by a standard inversion recovery pulse sequence with both $\{^1H\}$NOE and decoupling (broadband and selective decoupling for the diamagnetic $[Lu(do3ap^{Me})]^-$ and paramagnetic $[Yb(do3ap^{Me})]^-$ complexes, respectively). All experiments were run on a Bruker Avance III 600 spectrometer with a broadband probe (150 MHz for ^{13}C) due to the increased Curie contribution to the paramagnetic relaxation at higher fields. The ^{13}C T_2* relaxation times of the C=O groups in the $[Yb(do3ap^{Me})]^-$ complex were determined from the widths of the signals at half height after deconvolution of the signals in MestReNova©. For the $-CH_3$ group, ^{13}C T_2* relaxation time is not well defined due to its *J*-splitting and the ^{13}C T_2 value determined by the standard CPMG sequence was used instead. All experiments were measured at the complex concentration of c_M ~50 mM due to the observation of intermolecular contributions to relaxation at higher concentrations, similarly to that observed for the analogous H_4dota complexes[15]. For both inversion recovery and CPMG, 20 points were measured and then integral intensities *I* were determined in MestReNova© and the data were fitted to Equations (S1) and (S2), respectively, in Matlab®.

$$I = a - b\,e^{-t/T_1} \quad \text{(S1)}$$

$$I = c\,e^{-t/T_2} \quad \text{(S2)}$$

Determination of concentration in paramagnetic samples by the Evans method

Concentrations of the paramagnetic Ln^{III} complexes in NMR samples (shown in **Tables S13–S15**) were determined from the bulk magnetic susceptibility of the samples using the ^{1}H NMR chemical shift difference of *t*BuOH methyl signal in the paramagnetic solution and in the diamagnetic D_2O solution in a coaxial insert tube, Δδ. The concentration of paramagnetic Ln^{III}, c_{Ln}, was calculated from the difference Δδ according to Equation (S3).

$$c_{\mathrm{Ln}} = \frac{2{,}84^2 \cdot T \cdot \Delta\delta}{4\pi \cdot \left(\frac{1}{3} - \alpha\right) \cdot \mu_{\mathrm{eff}}{}^2} \qquad \text{(S3)}$$

Here, α is the demagnetisation factor, which is α = 0 for cylindrical samples parallel with the external magnetic field, and the μ_{eff} is the effective magnetic moment, considered constant for complexes of particular Ln^{III}. Values of μ_{eff} were taken from the literature[16] and are shown in **Table S13**.

Table S13: Effective magnetic moments of Ln^{III} from the literature[16] used for the determination of concentrations of paramagnetic complexes.

Ln	Ce	Pr	Nd	Sm	Eu	Gd	Tb	Dy	Ho	Er	Tm	Yb
μ_{eff} [BM]	2.56	3.62	3.68	1.6	3.45	7.94	9.7	10.6	10.6	9.6	7.6	4.5

Synthesis of non-labelled H_4do3ap^{Me}

The non-labelled H_4do3ap^{Me} was prepared from methyl-dichlorophosphine and a macrocylic precursor tBu$_3$do3a according to the **Scheme S1**. The *i*-propyl ester was used due to its higher chemical stability compared with ethyl or methyl esters.

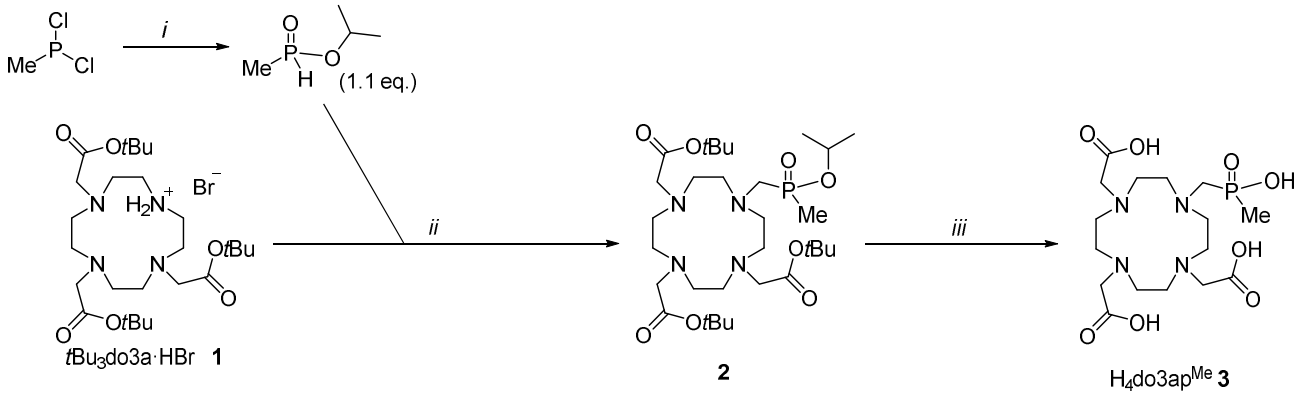

Scheme S1. Synthesis of the non-labelled H_4do3ap^{Me}: (*i*) *i*PrOH (2.25 equiv.), anhydrous pyridine (1 equiv.), THF, 0 °C→ r.t., 12 h; (*ii*) paraformaldehyde (4 × 3.3 equiv.), pyridine, 40 °C, 4 × 24 h; (*iii*) 6 M aq. HCl, 80 °C, 24 h.

Isopropyl methyl-H-phosphinate. An apparatus consisting of a 250-ml three-necked flask and a dropping funnel was heated and cooled under an argon atmosphere to remove moisture from the glass surface. Under argon atmosphere, solution of anhydrous *i*PrOH (2.1 ml, 1.6 g, 27 mmol) and anhydrous pyridine (1.0 ml, 0.98 g, 12 mmol) in anhydrous THF (50 ml) was added dropwise to a solution of CH_3PCl_2 (1.1 ml, 1.5 g, 12 mmol) in anhydrous THF (40 ml) in the 250-ml three-necked flask with intense stirring and cooling of the reaction mixture to 0 °C. Pyridinium hydrochloride was formed as a white solid during the addition of the *i*PrOH/pyridine mixture. The mixture was allowed to warm to room temperature while stirring for 12 h. Progress of the reaction was monitored by ^{31}P NMR (multiplet at approx. 28 ppm). After 12 h, the precipitate was filtered off on a fine glass frit and washed with THF (2 × 15 ml). The filtrate was concentrated *in vacuo* to a nearly complete evaporation of THF. **However, a prolonged evaporation *in vacuo* had to be avoided due to a partial evaporation of the product!** The residue was dissolved in EtOAc and the mixture was purified by column chromatography (SiO_2, 50 g, impurities were eluted by EtOAc and the product was eluted by *i*PrOH, R_f(*i*PrOH) ≈ 0.5). After evaporation of volatiles from the combined product-containing fractions, the *i*-propyl methyl-*H*-phosphinate was obtained as a clear liquid (1.1 g, 72 % with respect to $MePCl_2$).

^{1}H NMR (400 MHz, $CDCl_3$, 25 °C) δ: 1.29 (d, $^3J_{HH}$ 6.1 Hz, 3H, OCH(C$\underline{H}_3$)$_2$), 1.33 (d, $^3J_{HH}$ 6.1 Hz, 3H, OCH(C$\underline{H}_3$)$_2$), 1.47 (dd, $^2J_{PH}$ 15.1 Hz, $^3J_{HH}$ 2.1 Hz, 3H, $\underline{H}_3$CP), 4.60 (dheptd, $^3J_{PH}$ 9.4 Hz, $^3J_{HH}$ 6.1 Hz, $^4J_{HH}$ 0.9 Hz, 1H, OC$\underline{H}$(CH$_3$)$_2$), 7.21 (dqd, $^1J_{PH}$ 535 Hz, $^3J_{HH}$ 2.1 Hz, $^4J_{HH}$ 0.8 Hz, 1H, H$_3$C–P($\underline{H}$)(O)O*i*Pr). ^{13}C{^{1}H} NMR (101 MHz, $CDCl_3$, 25 °C) δ: 15.52 (d, $^1J_{CP}$ 96.0 Hz, H$_3\underline{C}$P(H)(O)O*i*Pr), 23.36 (d, $^3J_{CP}$ 4.4 Hz, OCH(C$\underline{H}_3$)$_2$), 24.31 (d, $^3J_{CP}$ 4.4 Hz, OCH(C$\underline{H}_3$)$_2$), 70.99 (d, $^2J_{CP}$ 6.4 Hz, O$\underline{C}$H(CH$_3$)$_2$). ^{31}P NMR (162 MHz, $CDCl_3$, 25 °C) δ: 31.0 (dqd, $^1J_{PH}$ 535 Hz, $^2J_{PH}$ 14.9 Hz, $^3J_{PH}$ 9.9 Hz).

MS (ESI$^+$): *m/z* 145.1 (145.0) [M + Na]$^+$. TLC (*i*PrOH): R_f 0.5.

Compound 2. The *t*Bu$_3$do3a·HBr **1** (5.0 g, 8.4 mmol) and *i*-propyl methyl-*H*-phosphinate (1.1 g, 9.0 mmol) were dissolved in pyridine (200 ml) in a 250-ml round-bottom flask. Paraformaldehyde (0.81 g, 27 mmol) was added to this solution, and the reaction mixture was stirred at 40 °C for 4 d. After each 24 h, more formaldehyde (≈0.25 g, 8.3 mmol) was added. The conversion was monitored by HPLC-MS. After the quantitative conversion of *t*Bu$_3$do3a·HBr, volatiles were evaporated *in vacuo*. The residue was dissolved in toluene (100 ml) and washed with 20% aq. K_2CO_3 (2×100 ml) and water (100 ml). The organic phase was dried with Na_2SO_4, the drying agent was filtered off on a glass frit and washed with toluene (50 ml). The volatiles were evaporated from the filtrate *in vacuo* to obtain the compound **2** (5.1 g, 92 % with respect to **1**).

^{1}H NMR (400 MHz, $CDCl_3$) δ: 1.29 (dd, $^3J_{HH}$ 6.2 Hz, $^4J_{PH}$ 3.3 Hz, 6H, OCH(C$\underline{H}_3$)$_2$), 1.43 (s, 27H, C(O)OC(C$\underline{H}_3$)$_3$), 1.54 (d, $^2J_{PH}$ 13.8 Hz, 3H, $\underline{H}_3$CP), 2.62–3.10 (m, 18H, NC$\underline{H}_2$C$\underline{H}_2$N and NC$\underline{H}_2$P), 3.20–3.55 (bs, 6H, NC$\underline{H}_2$COO*t*Bu), 4.68 (dhept, $^3J_{PH}$ 8.4 Hz, $^3J_{HH}$ 6.2 Hz, 1H, OC$\underline{H}$(CH$_3$)$_2$). ^{13}C{^{1}H} NMR (101 MHz, $CDCl_3$) *δ*: 15.34 (d, $^1J_{CP}$ 88.1 Hz, H$_3$C$\underline{P}$), 24.44 (d, $^3J_{CP}$ 3.7 Hz, POCH(C$\underline{H}_3$)$_2$), 24.73 (d, $^3J_{CP}$ 3.8 Hz, POCH(C$\underline{H}_3$)$_2$), 28.19 and 28.21 (C(O)C(C$\underline{H}_3$)$_3$), 50.98, 51.40 and 51.90 (N$\underline{C}$H$_2$C$\underline{H}_2$N), 52.13 (d, $^3J_{CP}$ 5.6 Hz, NCH$_2$C$\underline{H}_2$NCH$_2$P), 53.92 (d, $^1J_{CP}$ 103 Hz, NCH$_2$CH$_2$N$\underline{C}$H$_2$P), 55.98 (N$\underline{C}$H$_2$COO*t*Bu), 69.77 (d, $^2J_{CP}$ 6.9 Hz, O$\underline{C}$H(CH$_3$)$_2$), 82.44 and 82.48 (C(O)O$\underline{C}$(CH$_3$)$_3$), 169.22 and 169.3 ($\underline{C}$(O)OC(CH$_3$)$_3$). ^{31}P NMR (162 MHz, $CDCl_3$) *δ*: 49.3–49.8 (m).

MS (ESI$^+$): *m/z* 649.6 [M+H]$^+$, 671.6 [M+Na]$^+$. TLC (EtOH–conc. aq. NH_3 35:1): R_f 0.6.

Compound 3 (H$_4$do3ap^{Me}). In a 250-ml round-bottom flask, compound **2** (5.1 g, 7.9 mmol, 1 equiv.) was dissolved in aq. HCl (≈6 M, ≈150 ml) and stirred at 80 °C for 24 h. The volatiles were evaporated *in vacuo*. The residue was dissolved in a minimal amount of water (10 ml), and the mixture was purified on a strong cation-exchange resin (Dowex 50W×4, 6×80 cm resin bed, H$^+$-form). First, the resin was washed with water until the pH of the eluate was neutral. Then, the product was eluted off with 10% aq. pyridine (approx. 300 ml). The pyridine fractions containing the pure ligand were unified and volatiles were evaporated *in vacuo*. To remove pyridine, the oily residue was dissolved in a minimal amount of water, and the solution was passed through a weak cation-exchange resin (Amberlite CG50, 6×4 cm resin bed, H$^+$-form). The resin was washed with water (approx. 600 ml), and volatiles were evaporated from the filtrate. The residual pyridine was removed by co-evaporation with water *in vacuo*. Then, the residue was dissolved in a minimal amount of MeOH (10 ml) containing 0.5% H_2O, and the product was isolated by an addition of EtOH (20 ml) followed by an addition of Et_2O (50 ml). The precipitate was filtered off on a fine glass frit, washed with Et_2O (5×10 ml) and dried in an oven at 80 °C for 15 min. The product was isolated as a white powder with the composition of H$_4$do3ap^{Me}·2H$_2$O (2.9 g, 73 % based on *t*Bu$_3$do3a·HBr).

^{1}H NMR (300 MHz, D$_2$O/CsOD, pD ~13.5) δ: 1.28 (d, $^2J_{PH}$ 13.1 Hz, 3H, CH$_2$P(O)(OH)C$\underline{H}_3$), 2.78 (d, $^2J_{PH}$ 7.9 Hz, 2H, NC$\underline{H}_2$P(O)(OH)CH$_3$), 2.85 až 3.02 (m, 16H, NC$\underline{H}_2$C$\underline{H}_2$N), 3.29 (s, 2H, NC$\underline{H}_2$COOH), 3.33 (s, 4H, NC$\underline{H}_2$COOH). ^{13}C{^{1}H} NMR (101 MHz, D$_2$O, pD ~13.5) δ: 17.14 (d, $^1J_{CP}$ 88.7 Hz, CH$_2$P(O)(OH)$\underline{C}$H$_3$), 50.33, 51.18 & 51.21 (N$\underline{C}$H$_2$C$\underline{H}_2$N), 51.50 (d, $^3J_{CP}$ 4.7 Hz, NCH$_2$C$\underline{H}_2$NCH$_2$P), 56.27 (d, $^1J_{CP}$ 98.9 Hz, N$\underline{C}$H$_2$P(O)(OH)CH$_3$), 58.45 & 58.59 (N$\underline{C}$H$_2$COOH), 178.45 & 179.01 (NCH$_2$$\underline{C}$OOH). ^{31}P NMR (121 MHz, D$_2$O, pD ~13.5) δ: 40.0 (qt, $^2J_{HP}$ 13.2 Hz, $^2J_{HP}$ 8.1 Hz).

MS (ESI$^+$): *m/z* 439.3 ([M+H]$^+$, 461.3 [M+Na]$^+$. TLC (EtOH–conc. aq. NH_3 2:1): R_f 0.45. Elem. analysis: found (required for H$_4$do3ap^{Me}·2H$_2$O): C 40.86 (40.51), H 7.10 (7.44), N 11.86 (11.81), P 6.0 (6.53).

Synthesis of ^{17}O-enriched ethyl methyl-H-phosphinate

The ^{17}O-enriched ethyl methyl-*H*-phosphinate was prepared *in situ* by hydrolyzing the $MePCl_2$ with the ^{17}O-enriched water, followed by an alkylation with $(Et_3O)[BF_4]$ (**Scheme 1** in the main text).

^{17}O-labelled methyl-H-phosphinic acid. In an argon atmosphere in a pre-dried glass apparatus, $MePCl_2$ (0.75 ml, 1.0 g, 8.6 mmol, containing approx. 5 $\%_{mol}$ PCl_3) dissolved in anhydrous THF (40 ml) was added dropwise to the solution of ^{17}O-enriched water (400 µl, approx. 12 % ^{17}O) in anhydrous THF (40 ml) in a 100-ml two-necked flask while stirring intensively and cooling the mixture to 0 °C. This mixture was stirred for 12 h while the mixture was allowed to warm to room temperature. Volatiles were evaporated *in vacuo* to dryness. The crude product was purified by column chromatography (SiO_2, 50 g, elution by conc. aq. NH_3/EtOH 1:10, R_f (product) = 0.5 and R_f (H_3PO_3, main impurity) = 0). The volatiles were evaporated from the pure product-containing fractions at reduced pressure to obtain the ammonium salt of the product. The residue was dissolved in water and applied to a column of strong cation exchange resin Dowex 50W×4 (H^+-form, 4×10 cm). The product was eluted from the resin by water until the pH of the eluate was neutral. Volatiles from the combined product-containing fractions were evaporated *in vacuo*. The residue was dissolved in CH_2Cl_2 (cca 50 ml), and this solution was dried with anhydrous Na_2SO_4. The drying agent was filtered off and washed with CH_2Cl_2 (3×10 ml). The volatiles were evaporated from the filtrate to obtain the product as a clear liquid in 0.58 g (85 %) yield. The ^{1}H, ^{13}C and ^{31}P NMR agreed with the literature.[17]
^{17}O NMR (54 MHz, D_2O, pD ~2.4) δ: 94 (d, $^1J_{OP}$ 105 Hz).

^{17}O-labelled ethyl methyl-H-phosphinate. The 25-ml Schlenk flask was heated and left to cool under argon atmosphere. Then, $(Et_3O)[BF_4]$ (3.7 g, 19 mmol) was added to the flask and dissolved in anhydrous CH_2Cl_2 (12 ml). Under argon atmosphere, a solution of ^{17}O-labelled methyl-*H*-phosphinic acid (0.58 g, 7.3 mmol) in anhydrous CH_2Cl_2 (4 ml) was added dropwise to the solution of $[Et_3O][BF_4]$ under intense stirring and while cooling by ice/water bath to 0 °C. Subsequently, a solution of 2,6-lutidine (1.6 ml, 1.5 g, 14 mmol) in anhydrous CH_2Cl_2 (4 ml) was added dropwise to the reaction mixture during intense stirring and cooling to 0 °C by ice/water bath. After the additions, the ice/water bath was removed, and the mixture was stirred at room temperature for 3 h. After this time, the conversion was 100 % as confirmed by ^{31}P NMR (δ ≈ 34 ppm), which agreed with the literature.[18] The solution of ethyl methyl-*H*-phoshinate in CH_2Cl_2 was used in the subsequent reaction without isolating the product due to its volatility and instability to oxidation.

Comment: The 2,6-lutidine was used as a base here to prevent the alkylation of the phosphorus atom with stronger bases, which was confirmed by the appearance of a singlet in the ^{31}P NMR spectrum. This method was also successfully used in reactions with a compound containing a P–H bond previously[19]. This method of ester preparation by alkylation was chosen due to the preservation of ^{17}O enrichment, unlike most other methods of ester preparation. However, *i*-propyl methyl-*H*-phosphinate was used for the preparation of non-labelled H_4do3ap^{Me} as the bulky *iso*propyl group prevented the unwanted side reactions, mainly an oxidation of the P–H bond accompanied by an *N*-alkylation of the macrocycle amine group, *i.e.,* reductive amination, as well as ester hydrolysis. As no method for the preparation of *i*-propyl methyl-*H*-phosphinate keeping the ^{17}O labelling could be devised, the ethyl methyl-*H*-phosphinate had to be used, but it led to a significantly lower yield due to the side reactions.

Preparation of the [Ln(do3ap^{Me})]$^-$ complexes. Complexes were prepared following this general procedure. The H_4do3ap^{Me}·2H_2O (approx. 30–40 mg, 1.1 equiv.) and $LnCl_3$·xH_2O (1 equiv.) were dissolved in water and the pH was changed to 7–8 by 0.5% aq. LiOH. The mixture was stirred at 60 °C for 3 days. Then, the volatiles were evaporated at reduced pressure and residual water was co-evaporated off with MeOH. The residue was dissolved in MeOH, and the complex was precipitated by slow addition of Et_2O (approx. 30 ml). The precipitate was washed with Et_2O (3×10 ml) and dried in an oven (60 °C, 15 min), yielding approx. 50–60 mg (80–95% based on $LnCl_3$·*x*H_2O and assuming the Li[Ln(do3ap^{Me})(H_2O)] composition). The complexes contained a very small excess of free H_4do3ap^{Me}, which does not interfere with the following measurements and guarantees the absence of free Ln^{III} ions. The ^{17}O-labelled complexes were prepared analogously from the ^{17}O-labelled H_4do3ap^{Me}. Samples for the NMR measurements were prepared by dissolving the complexes (approx. 50 mg) in D_2O (approx. 0.5 ml)

Characterization of the complexes [Ln(do3ap^{Me})]$^-$:

TLC (*i*-PrOH–conc. aq. NH_3–H_2O 5:1:4): R_f (Ln = La – Er) ~0.7, R_f (Ln = Tm, Yb, Lu) ~0.6.

MS (ESI$^-$, only the most intensive signal(s) – ^{16}O and the most abundant Ln isotope(s) are listed; theoretical values and composition are in brackets): 573.2 (573.1, [^{139}La(do3ap^{Me})]$^-$); 574.2 (574.1, [^{140}Ce(do3ap^{Me})]$^-$); 575.1 (575.1, [^{141}Pr(do3ap^{Me})]$^-$); 576.1 & 578.3 [576.1/578.3, $^{142/144}$Nd(do3ap^{Me})]$^-$; 586.1 & 588.1 (586.1/588.1, [$^{152/154}$Sm(do3ap^{Me})]$^-$); 585.1 & 587.3 (585.1/587.3, [$^{151/153}$Eu(do3ap^{Me})]$^-$); 590.0, 591.9 & 594.7 (590.1/592.1/594.1, [$^{156/158/160}$Gd(do3ap^{Me})]$^-$); 593.3 (593.1, [^{159}Tb(do3ap^{Me})]$^-$); 596.3, 597.2 & 598.2 (596.1/597.1/598.1, [$^{162/163/164}$Dy(do3ap^{Me})]$^-$); 599.3 ([599.1, ^{165}Ho(do3ap^{Me})]$^-$); 600.1 & 601.6 (600.1/602.1, [$^{166/168}$Er(do3ap^{Me})]$^-$); 603.0 (603.1, [^{169}Tm(do3ap^{Me})]$^-$); 607.9 (608.1, [^{174}Yb(do3ap^{Me})]$^-$); 609.2 (609.1, [^{175}Lu(do3ap^{Me})]$^-$).

NMR: The ^{1}H signals of axial (paramagnetic samples) or methyl (diamagnetic samples) protons are listed in **Table S14**. For the definition of axial hydrogens, see SI of a reference[1]. The ^{31}P and ^{17}O NMR signals are listed in **Tables S15–S16**. The corresponding spectra are shown in **Figures S4–S9**.

Table S14. The ^{1}H NMR shifts of axial proton signals in the paramagnetic [Ln(do3ap^{Me})]$^{-}$ complexes and of methyl proton signals in the diamagnetic [Ln(do3ap^{Me})]$^{-}$ complexes (D_2O, 5 °C, pD ~6.5, 600 MHz).

Ln^{III}	c_{Ln} [mM]	^{1}H NMR δ [ppm]			
		h-TSA/TSA′	*v*-TSA/TSA′	*v*-SA	*h*-SA
La^{III}	≈140	1.48 (d, $^{2}J_{PH}$ 14.3 Hz)[a]		–[b]	
Ce^{III}	81	−12.1, −8.4, −8.3, −7.4	−13. 7, −10.4, −6.8, −6.3	–[b]	–[b]
Pr^{III}	113	−47.6, −45.0, −27.3[c]	−38.0, −31.9, −21.3, −19.1	−53.5, −50.5, −48.0, −36.0	–[b]
Nd^{III}	121	−21.9, −14.9, −11.1, −5.3	−15.3, −11.6, −8.4, −6.1	−27.7 (2×)[c], −25.0, −21.6	−31.5, −28.0, −26.5[c]
Sm^{III}	114	–[d]	–[d]	−3.5 (2 ×)[c], −2.8,−1.8	–[d]
Eu^{III}	123	10, 12, 17, 21	10, 13, 18, 24	30, 36, 40, 41	30, 35, 39, 40
Tb^{III}	119	−389, −328, −242, −240	−298, −218, −206[c]	−473, −451, −427, −350	−468, −443, −408, −347
Dy^{III}	103	–[b]	−503, −427, −297, −271	−587, −532, −518, −383	−581, −494, −456, −404
Ho^{III}	131	–[b]	−248, −185, −161, −112	−293, −282, −257, −217	–[b]
Er^{III}	115	–[b]	147, 196[c], 213[c], 235	196[c], 213[c], 289, 299	–[b]
Tm^{III}	104	536, 631, 685[c]	555, 574, 636, 701	431 (2×)[c], 515, 543	394, 462, 495[c]
Yb^{III}	93	51, 72, 98, 123[c]	54, 74, 99, 126	129, 163, 173, 186	133, 147, 154, 176
Lu^{III}	≈140	1.19 (d, $^{2}J_{PH}$ 14.7 Hz)[a]		–[b]	

[a]Signals of *vertical* and *horizontal* diastereoisomers not resolved. [b]Signals of the particular isomer not detected or resolved. [c]Signals of some axial protons overlap. [d]Signals of axial protons were indistinguishable from other signals.

Table S15. The ^{31}P NMR chemical shifts of the [Ln(do3ap^{Me})]$^{-}$ complexes (D_2O, 5 °C, pD ~6.5, 243 MHz).

Ln^{III}	c_{Ln} [mM]	^{31}P NMR δ [ppm]			
		h-TSA/TSA′	*v*-TSA/TSA′	*v*-SA	*h*-SA
La^{III}	≈140	42.8[a]		–[b]	
Ce^{III}	81	34[a]		–[b]	
Pr^{III}	113	31	38	39[a]	
Nd^{III}	121	3.6	5.6	8.3[a]	
Sm^{III}	114	50	51	57	55
Eu^{III}	123	90	78	89	104
Tb^{III}	119	431	446	514[a]	
Dy^{III}	103	467	529	598	537
Ho^{III}	131	278[a]		317[a]	
Er^{III}	115	−81	−122	−47	10
Tm^{III}	104	−374	−411	−290	−225
Yb^{III}	93	−40	−45	−86[a]	
Lu^{III}	≈140	47.2	45.4	42.3	40.0

[a]Signals of *vertical* and *horizontal* diastereoisomers were not resolved. [b]Signals of the isomer were not detected or resolved.

Table S16. The ^{17}O NMR chemical shifts of the $[Ln(do3ap^{Me})]^-$ complexes (25 °C, D_2O, pD ~6.5, 81 MHz). Coordinated and non-coordinated oxygen atoms are labelled as O^C and O^N, respectively.

Ln^{III}	c_{Ln} [mM]	^{17}O NMR δ [ppm]				
		TSA/TSA′ (O^N)	TSA/TSA′ (O^C)		SA (O^N)	SA (O^C)
			horizontal	*vertical*		*vertical* *horizontal*
La^{III}	≈140	156[a]	131[a]		–[b]	–[b]
Ce^{III}	81	133[a]	391[a]		–[a]	–[a]
Pr^{III}	113	147[a,c]	704[a,c]		147[a,c]	704[a,c]
Nd^{III}	121	118[a,c]	695[a,c]		118[a,c]	695[a,c]
Sm^{III}	114	98[a,c]	124[a,c]		98[a,c]	124[a,c]
Eu^{III}	123	105[a,c]	−868	−922	105[a,c]	−953[a]
Gd^{III}	126	101[a,c]	–[d]		101[a,c]	–[d]
Tb^{III}	119	249/254[e]	−2345[a]		249/254[b]	−2226[a]
Dy^{III}	103	278/292[e]	−1612[a]		278/292[b]	−1394[a]
Ho^{III}	131	200[a,c]	−1839[a]		200[a,c]	−1761[a]
Er^{III}	115	51[a,c]	−2082[a]		51[a,c]	−1963[a]
Tm^{III}	104	−80[a,c]	−1567[a,c]		−44[a,c]	−1567[a,c]
Yb^{III}	93	98[a,c]	−401[a]		71[a,c]	−586[a]
Lu^{III}	≈140	142[a,c]	122[a,c]		142[a,c]	122[a,c]

[a]Signals of *vertical* and *horizontal* diastereoisomers were unresolved. [b]Signals of the isomer were not detected or resolved. [c]Signals of the TSA a SA diastereoisomers were not resolved. [d]Signal of the coordinated oxygen atom was undetectable due to a fast relaxation. [e]Signals could not be assigned.

Definitions of matrices R and A

Matrices (matrix **R** containing rate constants and relaxation rates and matrix **A** containing integral intensities of cross-peaks and diagonal peaks divided by integral intensities I_0 at $\tau_m = 0$) used to determine rate constants of 2D ^{31}P–^{31}P EXSY (Equation (6) in the main text) are defined as follows.

$$\mathbf{R} = \begin{pmatrix} R_1^{\mathrm{SA}-B} - k_1 - k_5 - k_{11} & k_6 & k_{12} & k_2 \\ k_5 & R_1^{\mathrm{TSA}-B} - k_3 - k_6 - k_9 & k_4 & k_{10} \\ k_{11} & k_3 & R_1^{\mathrm{SA}-A} - k_4 - k_7 - k_{12} & k_8 \\ k_1 & k_9 & k_7 & R_1^{\mathrm{TSA}-A} - k_2 - k_8 - k_{10} \end{pmatrix}$$

$$\mathbf{A} = \begin{pmatrix} \frac{I(\mathrm{SA}-B)}{I_0(\mathrm{SA}-B)} & \frac{I(\mathrm{TSA}-B \rightarrow \mathrm{SA}-B)}{I_0(\mathrm{TSA}-B)} & \frac{I(\mathrm{SA}-A \rightarrow \mathrm{SA}-B)}{I_0(\mathrm{SA}-A)} & \frac{I(\mathrm{TSA}-A \rightarrow \mathrm{SA}-B)}{I_0(\mathrm{TSA}-A)} \\ \frac{I(\mathrm{SA}-B \rightarrow \mathrm{TSA}-B)}{I_0(\mathrm{SA}-B)} & \frac{I(\mathrm{TSA}-B)}{I_0(\mathrm{TSA}-B)} & \frac{I(\mathrm{SA}-A \rightarrow \mathrm{TSA}-B)}{I_0(\mathrm{SA}-A)} & \frac{I(\mathrm{TSA}-A \rightarrow \mathrm{TSA}-B)}{I_0(\mathrm{TSA}-A)} \\ \frac{I(\mathrm{SA}-B \rightarrow \mathrm{SA}-A)}{I_0(\mathrm{SA}-B)} & \frac{I(\mathrm{TSA}-B \rightarrow \mathrm{SA}-A)}{I_0(\mathrm{TSA}-B)} & \frac{I(\mathrm{SA}-A)}{I_0(\mathrm{SA}-A)} & \frac{I(\mathrm{TSA}-A \rightarrow \mathrm{SA}-A)}{I_0(\mathrm{TSA}-A)} \\ \frac{I(\mathrm{SA}-B \rightarrow \mathrm{TSA}-A)}{I_0(\mathrm{SA}-B)} & \frac{I(\mathrm{TSA}-B \rightarrow \mathrm{TSA}-A)}{I_0(\mathrm{TSA}-B)} & \frac{I(\mathrm{SA}-A \rightarrow \mathrm{TSA}-A)}{I_0(\mathrm{SA}-A)} & \frac{I(\mathrm{TSA}-A)}{I_0(\mathrm{TSA}-A)} \end{pmatrix}$$

In **R**, the R_1^X are longitudinal relaxation rates of the diastereoisomer *X* and $k_{1–12}$ are the rate constants of dynamic processes in the $[Eu(H_2O)(do3ap^{Me})]^-$ system as defined in Table S17. In **A**, the *I*(X) are integral intensities of diagonal peaks corresponding to diastereoisomers *X*, *I*(*X*→*Y*) are integral intensities of cross-peaks corresponding to chemical exchange from diastereoisomer *X* to diastereoisomer *Y* and the I_0(X) are integral intensities of diagonal peaks corresponding to diastereoisomers *X* at time $\tau_m = 0$.

Table S17: Definitions of rate constants in the $[Eu(H_2O)(do3ap^{Me})]^-$ complex.

k_1	Macrocycle inversion SA-*B*→TSA-*A*	k_2	Macrocycle inversion TSA-*A*→SA-*B*
k_3	Macrocycle inversion TSA-*B*→SA-*A*	k_4	Macrocycle inversion SA-*A*→TSA-*B*
k_5	Pendant arms re-orientation SA-*B*→TSA-*B*	k_6	Pendant arms re-orientation TSA-*B*→SA-*B*
k_7	Pendant arms re-orientation SA-*A*→TSA-*A*	k_8	Pendant arms re-orientation TSA-*A*→SA-*A*
k_9	Phosphinate rotation TSA-*B*→TSA-*A*	k_{10}	Phosphinate rotation TSA-*A*→TSA-*B*
k_{11}	Phosphinate rotation SA-*B*→SA-*A*	k_{12}	Phosphinate rotation SA-*A*→SA-*B*

Determination of kinetic parameters from VT ^{17}O NMR

The VT ^{17}O NMR spectra were fitted to the Equation (S4) describing a spectrum *S*(ω) for a two-site chemical exchange between two sites A and B (representing the coordinated and non-coordinated oxygen atom here). Here, M_0 is the initial magnetisation, R_j is the longitudinal relaxation time of site *j*, k_{ex} is the rate constant, ω_j is the resonance frequency of spin *j* and ω is the frequency. This equation is derived from Bloch-McConnel equations[20].

$$S(\omega) = M_0 \frac{R_A + R_B + 4k - i(\omega_A - \omega) - i(\omega_B - \omega)}{2[k + R_A - i(\omega_A - \omega)][k_{ex} + R_B - i(\omega_B - \omega)] - 2k^2} \quad \text{(S4)}$$

Natural chemical shifts of signals ω_j were determined from the chemical shifts at 0 °C. For the coordinated oxygen atoms of paramagnetic complexes, the expected change of these shifts with temperature due to the LIS was determined by fitting the values of chemical shift δ at low temperatures (0–15 °C) to Equation (S5), the Curie-Weiss approximation adequate for the temperatures in the range of 200–350 K.[21] The δ_{dia} and C are the diamagnetic shift and Curie constant, respectively, and both were determined by the fitting procedure.

$$\delta = \delta_{dia} + \frac{C}{T} \quad \text{(S5)}$$

For the non-coordinated oxygen atoms, natural chemical shifts were considered temperature-independent. Natural linewidths/longitudinal relaxation times of the signals were determined from the linewidths determined at 5 °C with an Arrhenius-type dependence (Equation (S6)) used to approximate the quadrupolar effects. In this equation, the pre-exponential factor w^{278} is the signal full width at half maximum at 278 K and E_A is a parameter corresponding to the activation energy for relaxation-causing motions, here determined by fitting the temperature dependence of ^{17}O NMR signal linewidths of the fully deprotonated ligand (pH ~14, set by a solid CsOH). This Arrhenius-type dependence should be a sufficient approximation for quadrupolar relaxation in the studied system and was successfully used in studies of similar Ln^{III} complexes.[12],[13],[22],[23]

$$w = w^{273} \cdot \exp\left(E_A\left(\frac{1}{T} - \frac{1}{273}\right)\right) \quad \text{(S6)}$$

The rate constants of phosphinate rotation were determined at each temperature for all the studied systems by fitting the spectrum to Equation (S4). Due to the simplified model used, all rate constants are a weighted average over all present diastereoisomers, and the 95% confidence intervals of their values were determined by repeating the fit with Gaussian distributed errors from multiple sources: the spectral noise and the errors of natural chemical shifts and linewidths determination.

Experimental for the X-ray diffraction studies

A single crystal of $H_4do3ap^{Me}\cdot 3H_2O$ was obtained by a slow diffusion of THF vapours into the solution of the unlabelled H_4do3ap^{Me} in MeOH/H_2O 1:2 (*v*/*v*) mixture. Single crystals of $[Li(H_2O)_3][Yb(do3ap^{Me})]\cdot H_2O$ and $[Li(H_2O)_3][Yb(do3ap^{OEt})]\cdot H_2O$ were obtained by a slow diffusion of acetone vapours into the solutions of the complexes in MeOH/H_2O 1:1 (*v*/*v*). The $[Yb(do3ap^{Me})]^-$ was prepared by the general procedure for the preparation of $[Ln(do3ap^{Me})]^-$ as described above. The $[Yb(do3ap^{OEt})]^-$ was prepared according to the literature.[1] Selected experimental data are shown in **Table S18**.

Table S18. Selected experimental data for X-ray diffraction studies of solid-state structures of H_4do3ap^{Me}, $3H_2O$ $[Li(H_2O)_3][Yb(do3ap^{Me})]\cdot H_2O$ and $[Li(H_2O)_3][Yb(do3ap^{OEt})]\cdot H_2O$.

Compound	$H_4do3ap^{Me}\cdot 3H_2O$	$[Li(H_2O)_3][Yb(do3ap^{Me})]\cdot H_2O$	$[Li(H_2O)_3][Yb(do3ap^{OEt})]\cdot H_2O$
Formula	$C_{16}H_{37}N_4O_{11}P$	$C_{16}H_{35}LiN_4O_{12}PYb$	$C_{17}H_{37}LiN_4O_{13}PYb$
M [g mol^{-1}]	492.46	686.43	716.45
Crystal system	monoclinic	monoclinic	monoclinic
Space group	$P2_1/n$	$P2_1/n$	$P2_1$/c
a [Å]	8.7824(3)	9.0666(4)	7.5126(9)
b [Å]	14.4066(4)	7.6453(3)	18.183(2)
c [Å]	18.3812(5)	34.5406(16)	18.809(3)
β [°]	96.4310(11)	91.9875(15)	93.596(5)
V [Å^3]	2311.04(12)	2392.81(18)	2564.3(5)
Z	4	4	4
Total reflections	4548	5441	6042
Observed reflections	4513	5435	5842
$R(I>2\sigma(I))$; R'(all data)	0.0660; 0.0662	0.0670; 0.0670	0.0771; 0.0804
$wR(I>2\sigma(I))$; wR'(all data)	0.1418; 0.1419	0.1634; 0.1634	0.1946; 0.1973
CCDC ref. no.	2470192	2470193	2470194

In the crystal structure of $H_4do3ap^{Me}\cdot 3H_2O$, some large electronic maxima were located near the phosphinate pendant arm and one of the neighbouring acetate groups. They were best refined as a superposition of phosphinate/acetate groups sharing the pivot nitrogen atoms N1 and N4. To ensure comparable thermal factors of atoms from both disordered parts (to have a reliable calculation of occupancy factors), EADP was used for all six pairs of closely lying atoms from both individual disordered parts. The disorder was refined with relative occupancies 87.8:12.2 %. For a substituent bound to the nitrogen atom N1, phosphinate-to-acetate occupancies are 87.8:12.2 %, whereas on the nitrogen atom N4, the occupancies are inverted. The hydrogen atoms bound to the carbon atoms were fixed in theoretical positions using U(H) = 1.2U(C), and those bound to nitrogen and oxygen atoms (including water molecules of crystallisation) were fully refined.

In the crystal structures of $[Li(H_2O)_3][Yb(do3ap^{Me})]\cdot H_2O$ and $[Li(H_2O)_3][Yb(do3ap^{OEt})]\cdot H_2O$, no disorder was found. However, both structures were found to be twins. In the case of $[Li(H_2O)_3][Yb(do3ap^{Me})]\cdot H_2O$, the structure

was refined as a 2-component perfect twin, whereas the structure of $[Li(H_2O)_3][Yb(do3ap^{OEt})]\cdot H_2O$ was found to be a two-component non-merohedral twin. The hydrogen atoms bound to the carbon atoms were fixed in theoretical positions and those belonging to the water molecules of crystallisation were fixed in the original positions using U(H) = 1.2U(C, O). Some strong difference maxima remained in the electron density map; however, they cannot be chemically interpreted as they are close to the central ytterbium(III) ion and reflect a low crystal quality (probably complicated multiple twinning with a low contribution of the other domains) leading to a relatively high R and wR indices.

References

[1] A. Svítok, J. Blahut, P. Urbanovský and P. Hermann, Dynamics of coordinated phosphonate group directly observed by ^{17}O NMR in lanthanide(III) complexes of a mono(ethyl phosphonate) DOTA analogue. *Chem. Eur. J.* **2024**, *30*, e202400970.

[2] K. Momma and F. Izumi, VESTA 3 for three-dimensional visualization of crystal, volumetric and morphology data, *J. Appl. Crystallogr.*, **2011**, *44*, 1272–1276.

[3] J. F. Desreux, Nuclear magnetic resonance spectroscopy of lanthanide complexes with a tetraacetic tetraaza macrocycle. Unusual conformation properties. *Inorg. Chem.* **1980**, *19*. 1319–1324.

[4] S. P. Babailov, E. N. Zapolotsky, A. I. Kruppa, P. A. Stabnikov, I. A. Godovikov, E. V. Bocharov and E. S. Fomin, Two types of conformational dynamics and thermo-sensor properties of praseodymium-DOTA by ^{1}H/^{13}C NMR. *Inorg. Chim. Acta* **2019**, *486*, 340–344.

[5] J. Blahut, P. Hermann, Z. Tošner and C. Platas-Iglesias, A combined NMR and DFT study of conformational dynamics in lanthanide complexes of macrocyclic DOTA-like ligands. *Phys. Chem. Chem. Phys.* **2017**, *19*, 26662–26671.

[6] A. Miao, R. Dekkers, K. B. S. S. Gupta, M. Overhand, R. Dasgupta and M. Ubbink, Rigidified and hydrophilic DOTA-like lanthanoid ligands: Design, synthesis, and dynamic properties. *Inorg. Chem.* **2023**, *62*, 3776–3787.

[7] E. N. Zapolotsky, Y. Qu, and S. P. Babailov, Lanthanide complexes with polyaminopolycarboxylates as prospective NMR/MRI diagnostic probes: peculiarities of molecular structure, dynamics and paramagnetic properties. *J. Inclusion Phenom. Macrocyclic Chem.* **2022**, *102*, 1–33.

[8] S. P. Babailov, P. V. Dubovskii and E. N. Zapolotsky, Paramagnetic lanthanides as magnetic resonance thermo-sensors and probes of molecular dynamics: Holmium-DOTA complex. *Polyhedron* **2014**, *79*, 277–283.

[9] S. P. Babailov and E. N. Zapolotsky, Tm-DOTA as responsive relaxation and shift probe for NMR local temperature monitoring at high magnetic fields. *Inorg. Chim. Acta* **2021**, *517*, 120153.

[10] V. Jacques and J. F. Desreux, Quantitative two-dimensional EXSY spectroscopy and dynamic behavior of a paramagnetic lanthanide macrocyclic chelate: YbDOTA (DOTA = 1,4,7,10-tetraazacyclododecane-*N*,*N*′,*N*″,*N*‴-tetraacetic acid). *Inorg. Chem.* **1994**, *33*, 4048–4053.

[11] S. Aime, A. Barge, M. Botta, M. Fasano, A. Danilo and G. Bombieri, Crystal structure and solution dynamics of the lutetium(III) chelate of DOTA. *Inorg. Chim. Acta* **1996**, *246*, 423–429.

[12] F. Mayer, C. Platas-Iglesias, L. Helm, J. A. Peters and K. Djanashvili, ^{17}O NMR and density functional theory study of the dynamics of the carboxylate groups in DOTA complexes of lanthanides in aqueous solution. *Inorg. Chem.* **2012**, *51*, 170–178.

[13] L. Fusaro and M. Luhmer, An oxygen-17 dynamic NMR study of the Pr-DOTA complex. *Dalton Trans.* **2014**, *43*, 967–972.

[14] B. Jagadish, G. L. Brickert-Albrecht, G. S. Nichol, E. A. Mash and N. Raghunand, On the synthesis of 1,4,7-tris(*tert*-butoxycarbonylmethyl)-1,4,7,10-tetraazacyclododecane. *Tetrahedron Lett.* **2011**, *52*, 2058–2061.

[15] S. Aime, L. Barbero, M. Botta and G. Ermondi, Determination of metal-proton distances and electronic relaxation times in lanthanide complexes by nuclear magnetic resonance spectroscopy. *J. Chem. Soc., Dalton Trans.* **1992**, 225–228.

[16] H. Gysling and M. Tsutsui, Organolanthanides and organoactinides. *Adv. Organomet. Chem.* **1971**, *9*, 361–395.

[17] M. S. Markoulides and A. C. Regan, Synthesis of a phosphinate analogue of the anti-tumour phosphate di-ester perifosine via sequential radical processes. *Org. Biomol. Chem.* **2013**, *11*, 119–129.

[18] J. M. Cross, N. Gallagher, J. H. Gill, M. Jain, A. W. McNeillis, K. L. Rockley, F. H. Tscherny, N. J. Wirszycz, D. S. Yufit and J. W. Walton, Pyridylphosphinate metal complexes: Synthesis, structural characterisation and biological activity. *Dalton Trans.* **2016**, *45*, 12807–12813.

[19] J. Zhang, E. Lambert, Z. F. Xu, J. Brioche, P. Remy and S. R. Piettre, From oxygen to sulfur and back: Difluoro-*H*-phosphinothioates as a turning point in the preparation of difluorinated phosphinates: Application to the synthesis of modified dinucleotides. *J. Org. Chem.* **2019**, *84*, 5245–5260.

[20] H. M. McConnell, Reaction rates by nuclear magnetic resonance. *J. Chem. Phys.* **1958**, *28*, 430–431.

[21] S. P. Babailov, Lanthanide paramagnetic probes for NMR spectroscopic studies of molecular conformational dynamics in solution: Applications to macrocyclic molecules. *Prog. Nucl. Magn. Reson. Spectrosc.* **2008**, *52*, 1–21.

[22] L. Fusaro, F. Mocci, R. N. Muller and M. Luhmer, Insight into the dynamics of lanthanide-DTPA complexes as revealed by oxygen-17 NMR. *Inorg. Chem.* **2012**, *51*, 8455–8461.

[23] L. Fusaro, G. Mameli, F. Mocci, M. Luhmer and G. Cerioni, Dynamic NMR of low-sensitivity fast-relaxing nuclei: ^{17}O NMR and DFT study of acetoxysilanes. *Magn. Reson. Chem.* **2012**, *50*, 152–158.